1 **<METHODOLOGY>**

2 **Combination of long-term $^{13}CO_2$ labeling and isotopolog profiling**
3 **allows turnover analysis of photosynthetic pigments in Arabidopsis**
4 **leaves**

5

6 Anh Thi-Mai Banh[1], Björn Thiele[1,2], Antonia Chlubek[1], Thomas Hombach[1], Einhard
7 Kleist[1], Shizue Matsubara[1]*

8

9 *Correspondence: s.matsubara@fz-juelich.de
10 [1]IBG-2: Plant Sciences, Forschungszentrum Jülich, 52425 Jülich, Germany
11 [2]IBG-3: Agrosphere, Forschungszentrum Jülich, 52425 Jülich, Germany

12

Abstract

14 **Background:** Living cells maintain and adjust structural and functional integrity by continual
15 synthesis and degradation of metabolites and macromolecules. The maintenance and
16 adjustment of thylakoid membrane involve turnover of photosynthetic pigments along with
17 subunits of protein complexes. Quantifying their turnover is essential to understand the
18 mechanisms of homeostasis and long-term acclimation of photosynthetic apparatus. Here we
19 report methods combining whole-plant long-term $^{13}CO_2$ labeling and LC-MS analysis to
20 determine the size of non-labeled population (NLP) of carotenoids and chlorophylls (Chl) in
21 leaf pigment extracts of partially ^{13}C-labeled plants.

22 **Results:** The labeling chamber enabled parallel $^{13}CO_2$ labeling of up to 15 plants of
23 *Arabidopsis thaliana* with real-time environmental monitoring ([CO$_2$], light intensity,
24 temperature, relative air humidity and pressure) and recording. No significant difference in
25 growth or photosynthetic pigment composition was found in leaves after 7-d exposure to normal
26 CO_2 (~400 ppm) or $^{13}CO_2$ in the labeling chamber, or in ambient air outside the labeling
27 chamber (control). Following chromatographic separation of the pigments and mass peak
28 assignment by high-resolution Fourier-transform ion cyclotron resonance mass spectrometry
29 (MS), mass spectra of photosynthetic pigments were analyzed by triple quadrupole MS to
30 calculate NLP. The size of NLP remaining after the 7-d $^{13}CO_2$ labeling was ~10.3% and ~11.5%
31 for all-*trans*- and 9-*cis*-β-carotene, ~21.9% for lutein, ~18.8% for Chl *a* and 33.6% for Chl *b*,
32 highlighting non-uniform turnover of these pigments in thylakoids. Comparable results were
33 obtained in all replicate plants of the $^{13}CO_2$ labeling experiment except for three that were
34 showing anthocyanin accumulation and growth impairment due to insufficient water supply
35 (leading to stomatal closure and less ^{13}C incorporation).

Conclusions: Our methods allow $^{13}CO_2$ labeling and estimation of NLP for photosynthetic pigments with high reproducibility despite potential variations in $[^{13}CO_2]$ between the experiments. The results indicate distinct turnover rates of carotenoids and Chls in thylakoid membrane, which can be investigated in the future by time course experiments. Since ^{13}C enrichment can be measured in a range of compounds, long-term $^{13}CO_2$ labeling chamber, in combination with appropriate MS methods, facilitates turnover analysis of various metabolites and macromolecules in plants on a time scale of hours to days.

Background

Living cells need maintenance to preserve structural and functional integrity. The maintenance involves breakdown, (re)synthesis and active transport of molecules such as proteins and membrane lipids. While turnover (continual replacement by degradation and synthesis) of macromolecules – proteins in particular – is costly for cells, it allows adjustments of biochemical machinery to environmental changes [1].

Plants have relatively low rates of protein turnover compared to bacteria. Early investigations on protein turnover using $^{14}CO_2$ labeling have indicated turnover rate of approx. $0.1 \sim 0.2$ d^{-1} in leaves of tobacco, bean, wheat and barley, whereas bacterial cells may have overall protein turnover of $1.2–1.4$ d^{-1} [1]. More recently, proteomic studies using ^{15}N labeling have determined degradation rate (K_D; equivalent to turnover rate in a steady state) of numerous proteins, showing the median of 0.08 d^{-1} and 0.11 d^{-1} in barley and Arabidopsis leaves, respectively [2, 3]. The proteome analysis also highlighted great variations in K_D among proteins. In Arabidopsis leaves, in which K_D was estimated for 1228 non-redundant proteins, $\sim$15% of the proteins had >0.22 d^{-1} whilst $\sim$13% had <0.055 d^{-1} [3]. Among high-turnover proteins detected in both barley and Arabidopsis are THI1 (1.65 d^{-1} and 1.93 d^{-1} in barley and Arabidopsis, respectively) and THIC (0.64 d^{-1} and 0.89 d^{-1}) in thiamine biosynthesis, and D1 protein (0.94 d^{-1} and 1.08 d^{-1}) in photosystem II (PSII) reaction center [2, 3]. THI1 and D1 are considered "suicide proteins" because THI1 is a single-use enzyme that serves as a co-substrate by donating a sulfur atom of a cysteine [4, 5] and D1 acts as a safety device that is sacrificed to protect the rest of PSII against photooxidative damage [6–8].

2

69 Given the costs of protein turnover, one may ask: Are high-turnover proteins worth the

70 benefits? Some attempts have been made to estimate the costs and benefits of D1 damage and

71 repair in oxygenic photosynthesis [9, 10]. The calculation depends on the definition of costs

72 (energy requirement for degradation and synthesis of protein and RNA, additional needs for N

73 and P, missed opportunity for photosynthesis) and the extent of photodamage. The latter, in

74 turn, is influenced by environmental conditions and efficacy of photoprotective mechanisms,

75 including thermal energy dissipation, scavenging of reactive oxygen species, alternative

76 electron transport pathways, state transitions and chloroplast movement [6, 9]. Should it be

77 necessary to replace pigments and lipids in the reaction center and core complex of PSII during

78 the D1 turnover, this would increase the costs of repair and maintenance [9]. A PSII core

79 complex harbors in total 35 chlorophyll *a* (Chl *a*) molecules, two pheophytins, 11 all-*trans*-β-

80 carotenes (β-Car), two plastoquinones, two haem irons and more than 20 lipids besides Mn, Ca,

81 Cl and bicarbonate [11]. We must also keep in mind that not only D1 but also other proteins

82 associated with photosynthesis, such as PetD of cytochrome b_6f complex and PIFI of chloroplast

83 NAD(P)H dehydrogenase complex, have relatively high K_D values (>0.5 d^{-1}) in Arabidopsis [8].

84 Previously we have shown the turnover of Chl *a* and all-*trans*-β-Car in leaves of Arabidopsis

85 plants under illumination [12, 13]. A 30-min pulse labeling with $^{14}CO_2$ resulted in rapid

86 incorporation of ^{14}C in these pigments, whereas Chl *b* and xanthophylls were not labeled

87 throughout the subsequent 10-h chase [12]. Treatment with lincomycin, an inhibitor of plastid

88 translation and thus D1 synthesis, quickly and strongly suppressed ^{14}C incorporation in Chl *a*,

89 and to a lesser extent also β-Car, suggesting a link to the D1 turnover [13]. Although detection

90 of radioactive ^{14}C is highly sensitive as well as selective, turnover rates could not be determined

91 in these studies due to the unknown number of $^{12}C/^{14}C$ substitution per molecule. For example,

92 if all C atoms of Chl *a* and β-Car are labeled with ^{14}C, a molecule of Chl *a* ($C_{55}H_{72}O_5N_4Mg$)

93 will have stronger radioactivity than a β-Car ($C_{40}H_{56}$). However, if Chl *a* is partially labeled, let

94 us say 20 C atoms out of 55, its radioactivity is only a half of fully labeled β-Car. Another

95 downside of our $^{14}CO_2$ labeling was the use of excised leaves to minimize radioactive wastes,

96 which restricted the duration of the pulse-chase labeling experiments [12, 13].

97 ^{13}C offers a good alternative to ^{14}C in these respects. ^{13}C is a stable, non-hazardous isotope

98 that can be detected and quantified by mass spectrometry (MS). For each compound, mass

99 spectra can show the relative abundance of individual isotopologs having different isotopic

100 compositions (e.g. $^{13}C_{55}$, $^{12}C_{35}^{13}C_{20}$, $^{12}C_{55}$ etc. for Chls), thus enabling the counting of non-

101 labeled and ^{13}C-labeled (fully or partially) molecules. As the first step to study turnover of

102 photosynthetic pigments, we established a liquid chromatography (LC)-MS analysis method

3

103 for isotopolog profiling of carotenoids. This method, recently described in [14] for lutein (Lut),

104 allows identification and quantification of isotopologs in ^{13}C-labeled leaf pigment extracts.

105 Similar methods are also needed for Chls and other carotenoids to analyze turnover of these

106 pigments in a single run. Furthermore, long-term whole-plant ^{13}CO$_2$ labeling is ideally

107 performed in a chamber, in which the environmental conditions can be controlled and

108 monitored during labeling experiments. Such a chamber will open up new possibilities for

109 turnover studies of many different compounds in plants.

110 Here we report a protocol of 7-d ^{13}CO$_2$ labeling in a chamber that was specially designed

111 and constructed for this type of experiments. We also describe the LC-MS analysis methods to

112 identify isotopologs and calculate non-labeled population (NLP) of β-Car, Chl *a* and Chl *b*

113 besides Lut in pigment extracts of ^{13}C-labeled leaves. With these methods of ^{13}CO$_2$ labeling

114 and isotopolog analysis at hand, turnover of photosynthetic pigments and other metabolites can

115 be studied in the future by time course experiments.

116

Methods

117

Plant material and growth conditions

118

119 Plants of *Arabidopsis thaliana* (Columbia-0) were grown in 300-mL plastic cups with lids

120 (Additional file 1; Fig. A1; Bürkle, Bad Bellingen, Germany) which tightly fit into holders of

121 the labeling chamber described below. After cups had been filled with moist soil

122 (Dachstaudensubstrat SoMi 513, Hawita, Vechita, Germany), 1–2 cm^3 of seed starting soil

123 (Pikier Erde, Blaster Einheitserdewerk, Fröndenberg, Germany) was put in the center of the top

124 soil where individual seeds were sown. Cotyledons grew out of the cup through a hole (3 mm

125 diameter) made in the center of the lid. The lid thus separated the aboveground from root system

126 and soil to minimize the impact of root and soil respiration on the CO$_2$ composition inside the

127 labeling chamber. The lid (except the hole) was covered with aluminum foil to suppress algal

128 growth on the soil surface. Two holes (~4.5 mm diameter; Additional file 1; Fig. A1) made in

129 the bottom of the cups allowed bottom watering.

130 Plants were cultivated in a climate chamber under 12 h/12 h light/dark, 23°C/18°C air

131 temperature and constant 60% relative air humidity. Illumination was provided by fluorescent

132 tubes (Fluora L36 W/77, Osram, Munich, Germany) which gave light intensity of ~100 µmol

133 photons m^{-2} s^{-1} at plant height. Care was taken to keep soil moisture by regular watering from

134 the bottom. Five weeks after sowing, 15 plants of similar projected leaf area (PLA, 14–16 cm^2)

135 were selected for a preliminary CO$_2$ experiment to develop a gas flow rate protocol (see below).

136 Plants were transferred to the labeling chamber installed in a separate climate chamber. After

137 the flow rate protocol had been established, a new batch of plants were cultivated in the same

138 way and 19 plants having 14–16 cm^2 PLA were selected for a $^{13}CO_2$ experiment (day 0 in

139 Additional file 1; Figs. A2, A3a). Of these, 15 were placed in the labeling chamber while the

140 remaining four plants stayed outside the labeling chamber (control).

141   The rosettes of the 19 plants were individually harvested after seven light/dark cycles in

142 $^{13}CO_2$ or ambient air (day 8 in Additional file 1; Figs. A2, A3b). The rosettes were quickly

143 photographed for visual documentation before freezing in liquid N_2 for pigment analysis.

144

145 Measurement of PLA

146 During plant cultivation, PLA was determined daily by using the Growscreen-FLUORO

147 method [15] or by taking a top-view image of the plants. In the latter case, a blue reference chip

148 (2 cm diameter) was placed next to the plant (Additional file 1; Figs. A2–A4) to facilitate pixel-

149 to-area conversion. Images were analyzed by ImageJ [16] to obtain PLA.

150

151 $^{13}CO_2$ labeling

152 We constructed a chamber for long-term $^{13}CO_2$ labeling of small plants such as Arabidopsis

153 (Fig. 1). It is equipped with the following control and measuring devices: four mass flow

154 controllers (MFC1–MFC4; EL-FLOW F-201CV-10K-RAR-00-V, F-200C-RFB-33-Z, F-

155 201C-RFB-33-V, F-201CV-100-RAR-00-Z, Bronkhorst Deutschland Nord, Kamen, Germany)

156 for CO_2-free air and CO_2, an infrared gas analyzer (IRGA; LI-840, LI-COR, Lincoln, NE, USA)

157 to measure [CO_2], a custom-made dew point trap cooled by a water bath (6°C; Julabo F32 MA,

158 JULABO Labortechnik, Seelbach, Germany) to reduce air humidity, four fans (8412 NGMV,

159 EBM papst, Mulfingen, Germany) in four corners to mix the air inside the chamber, five

160 temperature sensors (type K, mawi-therm Temperatur-Prozeßtechnik, Essen, Germany) placed

161 in four corners and at the center, and one sensor each for air humidity (DKRF400,

162 Driesen+Kern, Bad Bramstedt, Germany), light intensity (LI-190R, LI-COR) and pressure

163 (M260 Multisense, Setra Systems, Boxborough, MA, USA).

164   The labeling chamber has 15 airtight holders for plant cups described above (Fig. 2a). The

165 chamber can be closed with a glass cover (50 x 88 x 16 cm; L x W x H) (Fig. 2b). The connection

166 between the glass cover and the chamber body is sealed with polyurethane foam gaskets

167 (Armaflex AF/E 10 mm, Armacell, Münster, Germany). As this sealing is not airtight, a small

168 overpressure is needed inside the labeling chamber to prevent diffusion of ambient air from the

169 outside (see below). The overpressure results in air leakage and thus a loss of $^{13}CO_2$ from the

170 chamber through the glass cover sealing. A shallow plastic basin attached to the lower surface

of the chamber body can be filled with water through a tubing (Fig. 2b) without opening the chamber. When plant cups are put in the holders, the bottom of the cups touches the water in the basin, thus allowing bottom watering.

While the labeling chamber is in operation, two gas pumps (NMP830KVDCB and N 816 K_DC-B, KNF Neuberger, Freiburg, Germany) continuously circulate the internal air through bypasses that lead to LI-840 and the dew point trap (Fig. 1). The flow rates of the gas pumps were set to 1 L min^{-1} (to LI-840) and 14 L min^{-1} (to the dew point trap). The four MFCs are controlled by a custom-made computer program (made with LabVIEW 2014; National Instruments, Austin, TX, USA), which also visualizes environmental readings of the sensors in real time and records the data every minute. The flow rates of MFC2 (CO_2 or $^{13}CO_2$) and MFC3 (CO_2-free air prepared by filtering the ambient air through an industrial adsorption dryer KEN-MT 3800 MSTE; Parker Hannifin, Kaarst, Germany) were adjusted such that [CO_2] of ~400 ppm was maintained during the light period (Additional file 1; Fig. A5a–c). The mass flow of CO_2-free air (1 L min^{-1} or 2 L min^{-1}) created a small overpressure (~60 Pa or 160-170 Pa; Additional file 1; Fig. A5d) inside the labeling chamber compared to the outside (atmospheric pressure, ~101.3 kPa) to prevent diffusion of external air into the chamber. The amount of CO_2 injection was increased as the light intensity increased in the morning (see below for light intensity regime) and as the plants grew larger (Additional file 1; Fig. A5b). To keep daytime [CO_2] constant, the amount of CO_2 injection must be balanced with net CO_2 fixation of the plants, which depends on the genotype, size (leaf area) and development, as well as the conditions during cultivation and labeling.

We did not inject CO_2 during the dark period (except during 20-min equilibration immediately before the onset of light period; see below) while the flow of CO_2-free air was increased from 1 L min^{-1} to 2 L min^{-1} (Additional file 1; Fig. A5a, b) to minimize accumulation of respired CO_2 with unknown degree of ^{13}C labeling. As a result, nocturnal [CO_2] decreased to below 100 ppm (Additional file 1; Fig. A5c). Since plants were grown in the ambient air, we set the flow rate of CO_2-free air to 2 L min^{-1} during the first light period when light respiration of $^{12}CO_2$ was expected to dilute $^{13}CO_2$. The flow rate of CO_2-free air was reduced to 1 L min^{-1} during the subsequent light periods (presumably decreasing $^{12}CO_2$ in respiration) to lower the overpressure and thus reduce the loss of $^{13}CO_2$ from the labeling chamber. During the dark periods, the high flow rate of CO_2-free air and thus the high overpressure (Additional file 1; Fig. A5d) effectively blocked the diffusion of external air into the chamber. Should the overpressure exceed a given threshold (250 Pa in this study), a safety valve would open automatically to release the air from the chamber. This threshold, however, was never reached

6

during the experiments (Additional file 1; Fig. A5d). In addition to the high flow rate during the dark periods, the labeling chamber was flushed with CO_2-free air (MFC1; 10 L min^{-1} for 45 min) at the end of each dark period to get rid of nocturnal air containing respiratory CO_2 of unknown isotopic composition. The flushing was followed by 20-min equilibration with a fresh mixture of CO_2 (MFC4; 5 mL min^{-1}) and CO_2-free air (MFC1; 10 L min^{-1}) immediately before the onset of the light period. An outlet valve was automatically opened during flushing and equilibration to keep the overpressure low.

We conducted a preliminary experiment using normal CO_2 (purchased from Air Products, Hattingen, Germany) to establish a flow rate protocol (Additional file 1; Figs. A2, A6). This protocol was then used in the experiment with $^{13}CO_2$ (>99 atom %; Linde, Pullach, Germany). Since LI-840 has a very low sensitivity to $^{13}CO_2$ [17], the readings were low in the $^{13}CO_2$ experiment (Additional file 1; Fig. A6). Nevertheless, light/dark patterns of [CO_2] were highly reproducible in both CO_2 and $^{13}CO_2$ conditions, suggesting that the flow rate protocol provided similar [CO_2] inside the labeling chamber. It should be noted, however, that [CO_2] and [$^{13}CO_2$] may vary if the size and growth rate (and thus the total CO_2 assimilation) of the plants differ between the CO_2 and $^{13}CO_2$ experiments due to suboptimal selection of plants or occurrence of stressed plants (see below).

The labeling chamber was placed under LED lamps (L4A Series 10, HelioSpectra, Göteborg, Germany) in the climate chamber running with 12 h/12 h light/dark and constant 20°C and 60% relative air humidity. The intensity of LED lamps was increased or decreased in three steps at the beginning or at the end of the 12-h light period, respectively (Additional file 1; Fig. A7a). The light period started with 30-min dim light (~28 µmol photons m^{-2} s^{-1}), followed by an increase to ~115 µmol photons m^{-2} s^{-1} (60 min) and then to ~200 µmol photons m^{-2} s^{-1} (9 h) before returning to darkness in the reverse sequence. The light intensity shown in Additional file 1; Fig. A7a was measured by LI-190R mounted near the plant position P7 and P8 (see Figs. 1, 2) in the closed chamber (i.e., under the glass cover). Figure 2a illustrates light distribution in the open chamber measured at plant height using X1 optometer (Gigahertz-Optik, Türkenfeld, Germany). The mean intensity of the 15 plant positions was 238 µmol photons m^{-2} s^{-1} ±10% SD without the glass cover. Comparing the values measured at around P7 and P8 in the open and closed chamber, the glass cover apparently reduced the light intensity by ca. 25%. For the control plants outside the labeling chamber, the intensity of LED was set to the level similar to the condition in Additional file 1; Fig. A7a.

While the climate chamber had constant 20°C and 60% relative air humidity, illumination and plant transpiration raised the air temperature and humidity inside the closed labeling

chamber (Additional file 1; Fig. A7b, c). The air temperature increased to ~23°C during the light period and decreased to ~20.5°C during the dark period. Although the chamber has a dew point trap (Fig. 1), the capacity of the dew point trap was not enough to fully compensate for the transpiration of 15 growing plants of Arabidopsis; the air humidity gradually increased from ~55% to ~75% during the 7-d experiments even though the chamber was flushed daily and the flow rate of CO_2-free air was kept at 2 L min^{-1} during the dark periods.

The $^{13}CO_2$ labeling was stopped after seven light/dark cycles. The chamber was opened in the dim light at the beginning of the light period of day 8 to harvest the whole rosette of each plant. As opening the chamber inevitably exposes plants to ambient air, we collected all plants (also the control) during the 30-min dim-light period to minimize photosynthetic CO_2 fixation. The total amount of $^{13}CO_2$ used by the flow rate protocol (including daily flushing, equilibration and loss in addition to CO_2 assimilation of 15 plants) during the 7-d labeling was ca. 6.8 L.

Pigment extraction

The whole rosettes of Arabidopsis plants were individually frozen in liquid N_2 and ground to powder using pre-cooled mortar and pestle. They were stored at -80°C until pigment extraction.

About 40 or 80 mg of frozen leaf powder were quickly weighed with an analytical balance (Explorer Pro, OHAUS, Nänikon, Switzerland). Pigments were extracted by using the protocol described before [14]. The weighed frozen leaf powder was ground in 2 mL of chilled acetone under dim light and the homogenate was collected in a 2-mL reaction tube. After 5-min centrifugation at 16,100 rcf (5415D, Eppendorf, Wesseling-Berzdorf, Germany), the supernatant was filtered through a syringe filter (0.45 μm, Chromafil® AO-45/3, Macherey-Nagel, Düren, Germany) into a brown glass vial. All extracts were prepared shortly before injection into LC-MS instruments.

MS analysis

The LC-MS system consists of a Waters ACQUITY UPLC system and a Waters Xevo TQ-S triple quadrupole MS (hereafter TQ-MS). The LC-Fourier-transform ion cyclotron resonance-MS (hereafter FTICR-MS) consists of an Agilent 1200 series HPLC system and a hybrid linear ion trap FTICR-MS (LTQ FT Ultra, Thermo Fisher Scientific) equipped with a 7 Tesla magnet. Soft ionization was performed in positive ion mode by electrospray ionization (ESI in TQ-MS) or atmospheric pressure chemical ionization (APCI in FTICR-MS). For information about the instrument settings, see [14].

Chromatographic separation was done by a C30 silica column (ProntoSil 200-3-C30, 250 x 4.6 mm, 3 μm, Bischoff Chromatography, Leonberg, Germany) using the method described in [14]. Pigments were identified based on absorption spectra. Chromatograms were extracted at 440 nm and peak area integration was performed by MassLynx software (version 4.1, Waters) for TQ-MS data. To determine pigment concentration, the LC of the TQ-MS system was calibrated with pigment standards purchased from DHI LAB products (Hørsholm, Denmark): Lut, all-*trans*-α-Car, all-*trans*-β-Car, Chl *a* and Chl *b* as well as 9-*cis*-neoxanthin (Neo), violaxanthin (Vio), antheraxanthin (Anthera) and zeaxanthin (Zea). Carotenoid levels relative to Chl (Chl *a* + Chl *b*) were calculated in mmol mol^{-1} Chl. The de-epoxidation state (DES) of the xanthophyll-cycle pigments was defined as (Anthera + Zea) / (Vio + Anthera + Zea).

Mass spectra were obtained at the maximal intensity of the pigment peaks in ion chromatograms (FTICR-MS) or by manually selecting the regions around the maximal peak intensity (TQ-MS) using a full scan mode to cover mass-to-charge ratio (*m*/*z*) between 350 and 1000. Data were processed with MassLynx for TQ-MS and Xcalibur (version 2.0.7, Thermo Fisher Scientific) for FTICR-MS. We first analyzed one each of the ^{13}C-labeled and non-labeled (control) samples using both TQ-MS and FTICR-MS to assign mass peaks. The high mass accuracy of FTICR-MS allows assignment of mass peaks to distinct empirical formulae. The resolving power (full width at half maximum) of FTICR-MS was 100,000 at *m*/*z* 400. Based on the peak assignment of FTICR-MS, matching peaks were identified in the corresponding data of TQ-MS. All other samples were analyzed by TQ-MS using the same peak selection schemes.

Degree of ^{13}C labeling (DoL) and NLP of pigments

The base peak intensity (BPI) was calculated for each pigment isotopolog as follows [14]:

$$BPI_i = \frac{I_i}{I_{(max)}} \cdot 100 \qquad \text{Eqn. 1}$$

where BPI$_i$ is the base peak intensity of an isotopolog with i ^{13}C atoms, i the number of ^{13}C atoms in the isotopolog, I$_i$ the peak intensity of an isotopolog with i ^{13}C atoms, and I$_{(max)}$ the highest peak intensity of all isotopologs of the pigment.

The BPI$_i$ values were then normalized to the sum of BPI$_i$ of all isotopologs of the pigment.

$$BPI_{i(norm)} = \frac{BPI_i}{\sum_{i=0}^{n} BPI_i} \cdot 100 \qquad \text{Eqn. 2}$$

BPI$_{i(norm)}$ is the normalized base peak intensity of an isotopolog with i ^{13}C atoms and n is the number of C atoms in the pigment molecule (40 for carotenoids, 55 for Chls).

The DoL was calculated for each isotopolog as follows:

$$DoL_i = \frac{BPI_{i(norm)} \cdot i}{n} \qquad \text{Eqn. 3}$$

305   where DoL_i is the degree of ^{13}C labeling of an isotopolog with i ^{13}C atoms.

306   The overall DoL (ΣDoL) of the pigment can be obtained by adding up DoL_i of all isotopologs.

307    $$\Sigma DoL = \sum_{i=0}^{n} DoL_i \qquad\qquad \text{Eqn. 4}$$

308   We estimated the relative abundance of non-labeled pigment population (NLP), which can

309   be defined as the sum of $BPI_{i(norm)}$ of all non-labeled isotopologs. Due to natural abundance of

310   [13]C in the atmosphere (1.1%), isotopologs having a few ^{13}C atoms are always found in plant

311   extracts (Additional file 1; Fig. A8). These naturally ^{13}C-containing isotopologs were

312   considered "non-labeled".

313

314   Spike test of TQ-MS

315   Pigment recovery of the TQ-MS system was checked by spike tests. About 40 mg of frozen leaf

316   powder of a ^{13}C-labeled Arabidopsis plant were homogenized in 2 mL of chilled acetone. The

317   homogenate was then divided into two aliquots and 0.5 mL of pigment standards (Lut, all-*trans*-

318   β-Car and Chl *a*; all from DHI LAB products) of known concentrations were spiked in one

319   aliquot. Both aliquots were centrifuged and the supernatants filtered into brown glass vials as

320   described above. Following TQ-MS analysis of the pigment standards and the ^{13}C-labeled

321   Arabidopsis leaf pigment extract with and without spike (Additional file 1; Fig. A9), $BPI_{i(norm)}$

322   was calculated for the pigments using Eqn. 2. Because addition of non-labeled standards should

323   increase the relative abundance of non-labeled isotopologs in the spiked sample, recovery of

324   the added standards can be estimated from the ratio between the measured and the expected

325   increase in NLP of the spiked sample compared to the non-spiked sample.

326    $$Recovery = \frac{measured\ NLP\ increase}{expected\ NLP\ increase} \qquad\qquad \text{Eqn. 5}$$

327   The results of the spike tests are documented in Additional file 2; Table 1. The recovery was

328   95% or higher for all three pigments.

329

330   Reproducibility of ΣDoL and NLP

331   Technical reproducibility of ΣDoL and NLP was verified by repeated injections of a ^{13}C-labeled

332   Arabidopsis pigment extract into TQ-MS and analyzing ΣDoL and NLP in these data. The mean

333   values (±SD with n=3 for all-*trans*-βCar, Lut and Chl *a*, n=4 for Chl *b*) of ΣDoL and NLP thus

334   obtained for each pigment are summarized in Additional file 2; Table 2.

335

336   **Results**

337   [13]CO$_2$ treatment in the labeling chamber

338   The labeling chamber was first run with normal CO_2 to establish a flow rate protocol of CO_2

339   and CO_2-free air (see the description in Methods). This was necessary because LI-840, which

340   was connected to the labeling chamber (Fig. 1), measures $[CO_2]$ at the wavelength of ~4.26 μm

341   where $^{12}CO_2$ absorbs much more strongly than $^{13}CO_2$ (Additional file 1; Fig. A6) [17].

342   Subsequently, the $^{13}CO_2$ labeling experiment was conducted using the same protocol.

343   Figure A2 in Additional file 1 shows top-view images of the plants at the beginning (day 0)

344   and at the end of the experiment (day 8). Grown in the same conditions, the plants with similar

345   PLA looked very much alike on day 0. After seven light/dark cycles in the normal CO_2 or $^{13}CO_2$

346   conditions inside the labeling chamber, the plants were visually indistinguishable from the

347   control plants that stayed in the ambient air outside the labeling chamber. The chamber has 15

348   plant cup holders for simultaneous labeling (Fig. 2). All 15 plants of the $^{13}CO_2$ experiment are

349   shown in Additional file 1; Fig. A3. Three plants (P6, P13 and P15) grew less and showed

350   anthocyanin accumulation during the experiment (Fig. 2b); their plastic cups were not placed

351   deep enough in the holders, resulting in suboptimal watering and stomatal closure, and thus less

352   CO_2 fixation and growth. No sign of stress was recognized in other 12 plants. For comparison,

353   the pictures of 15 plants used in the preliminary experiment with normal CO_2 are shown in

354   Additional file 1; Fig. A4. Two plants (P9 and P11) were somewhat smaller at the end of the

355   preliminary experiment. Overall, however, growth and visual phenotype of the plants were

356   comparable between the $^{13}CO_2$ and normal CO_2 experiments.

357   Leaf pigment composition was analyzed in the 15 plants of the $^{13}CO_2$ experiment as well as

358   four control plants. The ^{13}C-labeled plants and non-labeled control were comparable regarding

359   leaf carotenoid and Chl contents (Fig. 3), except that two control plants had somewhat higher

360   DES of the xanthophyll-cycle pigments (Fig. 3d). Since the leaves were harvested under dim

361   light in the morning, all samples had high levels of Vio, some Anthera and only trace amounts

362   of Zea (Fig. 3b, c). The pigment composition did not systematically differ between the stressed

363   plants (P6, P13 and P15) and the rest.

364

365   Mass peak assignment and calculation of DoL and NLP

366   The substitution of ^{12}C (mass 12.000000) by ^{13}C (mass 13.003355) and *vice versa* can be

367   detected in molecules by MS analysis. In order to identify pigment isotopologs in mass spectra

368   of ^{13}C-labeled samples, mass peaks were assigned to empirical formulae by high-resolution

369   FTICR-MS. Matching peaks were then selected in the corresponding data of TQ-MS. Since

370   mass peak assignment of Lut is explained elsewhere [14], we describe below the procedures of

371   peak assignment and analysis focusing on β-Car and Chls. We could not analyze mass spectra

372 of Zea due to the low concentrations in the samples (Fig. 3b); peak assignment of Vio, Anthera

373 and Zea is outside the scope of this study. The mass peak assignment of Lut, however, can be

374 considered a proof of principle for these xanthophylls. The MS analysis of Neo was confronted

375 by co-eluting compounds.

376 Chromatographic separation of photosynthetic pigments was monitored at 440 nm (Fig. 4a).

377 The ion chromatograms presented in Fig. 4b–g were extracted at nominal mass of monoisotopic

378 pigment ions: $^{12}C_{40}$ for carotenoids and $^{12}C_{55}$ for Chls. Since ionization occurred in positive

379 mode, $[M+H]^+$ was the major quasi-molecular ion of Vio (Fig. 4b) and Chls (Fig. 4d, f). Lut

380 has strong tendency to lose water upon protonation [14, 18, 19], forming $[M+H–H_2O]^+$ as the

381 main quasi-molecular ion (Fig. 4e). Vio also gave rise to multiple dehydration products ($–H_2O$,

382 $–2H_2O$ or $–3H_2O$) but $[M+H]^+$ was still the most abundant ion. In contrast to xanthophylls, both

383 all-*trans* and 9-*cis* isomers of β-Car predominantly formed $[M]^+$ in TQ-MS (Fig. 4g) and

384 $[M+H]^+$ in FTICR-MS (see below).

385 Figure 5 collates mass spectra of all-*trans*-β-Car in the non-labeled and ^{13}C-labeled samples

386 analyzed by FTICR-MS and TQ-MS. Similar mass spectra, albeit with stronger backgrounds,

387 were also obtained for the less abundant 9-*cis*-β-Car (Additional file 1; Fig. A10). The mass

388 peaks of β-Car are clustered around *m/z* 536–537 in the non-labeled sample (Fig. 5a, b;

389 Additional file 1; Fig. A10a, b). After the 7-d $^{13}CO_2$ treatment, a second peak cluster comprising

390 ^{13}C-labeled isotopologs emerged at around *m/z* 575–576 (Fig. 5c, d; Additional file 1; Fig. A10c,

391 d). The peaks of ^{13}C-labeled isotopologs were much higher than the non-labeled ones,

392 indicating that the majority of β-Car, both all-*trans* and 9-*cis*, were newly synthesized during

393 the $^{13}CO_2$ treatment.

394 We selected the mass peaks of all-*trans*-β-Car isotopologs in the TQ-MS data (Additional

395 file 2; Tables A4, A6) as per the peak assignment of FTICR-MS in the non-labeled and ^{13}C-

396 labeled samples (Additional file 2; Tables A3, A5). Due to limited mass resolution, TQ-MS

397 cannot distinguish mass peaks of $[M]^+$ and $[M+H]^+$ ions when they have similar *m/z* values

398 following $^{12}C/^{13}C$ substitution (Δ mass = 1.003355) or protonation (Δ mass = 1.007276).

399 FTICR-MS, at the resolving power used (100,000 at *m/z* 400), could separate most of the β-Car

400 peaks in the ^{13}C-labeled cluster, while it failed to resolve a few peaks in the non-labeled cluster

401 (Additional file 2; Tables A3–A6). In case of overlap, peaks were regarded as the more

402 abundant form. Thus, overlapping peaks of $[M]^+$ and $[M+H]^+$ were considered $[M]^+$ in the TQ-

403 MS analysis and $[M+H]^+$ in the FTICR-MS analysis of β-Car. This led to a small overestimation

404 of β-Car ΣDoL by TQ-MS because $[M]^+$ has one more ^{13}C atom compared to $[M+H]^+$ at similar

405 *m/z* (e.g. $[^{12}C_{39}{}^{13}C\text{-M}]^+$ and $[^{12}C_{40}\text{-M+H}]^+$). Consequently, ΣDoL values of all-*trans*-β-Car were

slightly higher when calculated from the TQ-MS data (ca. 1.4% and 86.1% for non-labeled and ^{13}C-labeled sample, respectively) instead of the FTICR-MS data (ca. 1.2% and 84.2%) (Additional file 2; Tables A3–A6). Using the same peak assignment, we found comparable ΣDoL for 9-*cis*-β-Car shown in Additional file 1; Fig. A10: ca. 1.2% and 84.7% for non-labeled and ^{13}C-labeled sample by TQ-MS, ca. 1.0% and 82.1% by FTICR-MS. Note that the peaks of all-*trans*- and 9-*cis*-β-Car were not completely separated in the ion chromatogram (Fig. 4g), which may partly explain the similar ΣDoL of these isomers.

Next, we estimated the size of NLP based on the relative abundance of non-labeled β-Car isotopologs in the ^{13}C-labeled sample (i.e., the sum of $BPI_{i(\text{norm})}$ in the white cells of Additional file 2; Tables A5, A6). For calculation of NLP, it should not matter whether unresolved peaks of β-Car are considered $[M]^+$ or $[M+H]^+$ because the overlaps occurred exclusively within the non-labeled or the ^{13}C-labeled peak cluster. Nevertheless, TQ-MS gave a somewhat smaller NLP of all-*trans*-β-Car (ca. 10.3%) than FTICR-MS did (ca. 12.2%) (Additional file 2; Tables A5, A6). The same also applied to 9-*cis*-β-Car (ca. 11.5% and 14.3% by TQ-MS and FTICR-MS, respectively). NLP is always 100% in non-labeled control.

We followed the same procedure to assign the mass peaks of Lut. As already mentioned, $[M+H-H_2O]^+$ is the predominant ion of Lut (Fig. 6) [14, 18, 19]. FTICR-MS separated all mass peaks of Lut detected in non-labeled and ^{13}C-labeled samples (Additional file 2; Tables A7, A9), while TQ-MS showed overlaps between $[M]^+$ and $[M+H]^+$ in both non-labeled and ^{13}C-labeled *m/z* regions (Additional file 2; Tables A8, A10). Since the overlapping peaks in the TQ-MS data were considered $[M+H]^+$, ΣDoL of Lut was slightly underestimated by TQ-MS in both non-labeled and ^{13}C-labeled samples (ca. 1.0% and 74.1%, respectively) compared to FTICR-MS (ca. 1.3% and 75.0%) (Additional file 2; Tables A7–A10). Conversely, NLP was marginally overestimated by TQ-MS in the labeled sample (ca. 21.9% vs 21.0% by FTICR-MS).

Unlike carotenoids, which are made solely of C and H (carotenes) or C, H and O (xanthophylls), Chls also contain N and Mg. While natural abundance of ^{2}H (0.02%), ^{17}O (0.04%), ^{18}O (0.2%) and ^{15}N (0.4%) are all low, two stable isotopes of Mg (^{25}Mg 10%, ^{26}Mg 11%) exist in significant amounts in nature alongside the most abundant ^{24}Mg (79%). Peak assignment and analysis of Chl mass spectra must take into account Mg isotopes (^{24}Mg/^{25}Mg Δ mass = 1.000795; ^{24}Mg/^{26}Mg Δ mass = 1.997551) in addition to ^{12}C/^{13}C substitution and protonation. Furthermore, the number of possible formulae increases with increasing molecular mass. As a result, Chl mass spectra were difficult to analyze even by FTICR-MS. Moreover, formation of $[M+K]^+$ adduct was seen in both FTICR-MS and TQ-MS data of Chl *a* (Fig. 7), and TQ-MS data of Chl *b* (Fig. 8b, d). Some TQ-MS data also showed a trace of $[M+Na]^+$ in

440 ^{13}C-labeled samples. To simplify the analysis of Chl mass spectra, we focused on the $[M+H]^+$

441 ion of ^{24}Mg-Chl because ^{13}C labeling of Chl should be independent of the type of ion produced

442 by MS instruments and of the Mg isotope inserted in the protoporphyrin IX during Chl

443 biosynthesis. The relative contributions of ^{24}Mg-Chl, ^{25}Mg-Chl and ^{26}Mg-Chl to overlapping

444 mass peaks were calculated based on the natural abundance of these Mg isotopes. As the peaks

445 of non-labeled $[M+K]^+$ and ^{13}C-labeled $[M+H]^+$ were partly overlapping (Figs. 7c, d and 8d),

446 we estimated the intensity of non-labeled $[M+K]^+$ peaks from the intensity of non-labeled

447 $[M+H]^+$ peaks in the same data, assuming the relative abundance of $[M+K]^+$ and $[M+H]^+$ peaks

448 found in the non-labeled control (Figs. 7a, b and 8b). The intensity of non-labeled $[M+K]^+$ was

449 then subtracted from the overlapping peaks to obtain the intensity of ^{13}C-labeled $[M+H]^+$.

450   The peak assignment and calculation of Chl *a* and Chl *b* are summarized in Additional file

451 2; Tables A11–A18. For comparison, calculation is reported for both $[M+H]^+$ and $[M+K]^+$ ions

452 in the non-labeled control (Additional file 2; Tables A11, A12, A16). As expected, ΣDoL did

453 not substantially differ between the two ionization products ($[M+H]^+$ and $[M+K]^+$). Between

454 the two instruments, TQ-MS gave higher ΣDoL for both non-labeled and ^{13}C-labeled samples

455 compared to FTICR-MS; the values obtained in the labeled sample were ca. 67.3% and 70.4%

456 for Chl *a* (by FTICR-MS and TQ-MS; Additional file 2; Tables A13, A14) and ca. 54.9% and

457 57.5% for Chl *b* (Additional file 2; Tables A17, A18). The TQ-MS data underestimated NLP

458 of Chl *a* in the ^{13}C-labeled sample (ca. 18.8% and 20.7% by TQ-MS and FTICR-MS), whereas

459 their NLP values were similar for Chl *b* (ca. 33.6% and 33.0%).

460   Overall, ΣDoL and NLP were largely comparable between the TQ-MS and FTICR-MS data,

461 with deviations ranging between less than one and a few points after the 7-d ^{13}CO$_2$ labeling.

462 Also the technical reproducibility was high for both parameters (Additional file 2; Table A2).

463

464 Variations in ΣDoL and NLP among the 15 plants in the ^{13}CO$_2$-labeling experiment

465 We analyzed ΣDoL and NLP in all samples using TQ-MS. Figure 9a shows box plots of ΣDoL.

466 Three plants had lower ^{13}C enrichment in the pigments; these were P6, P13 and P15 that

467 displayed anthocyanin accumulation and reduced growth (Additional file 1; Fig. A3b). The

468 smallest plant (P13) had the lowest ΣDoL for all pigments. Apart from these three, the other

469 ^{13}C-labeled plants were similar in terms of ΣDoL (Fig. 9a). β-Car had the highest average ΣDoL

470 (86.5% ±2.2 SD for all-*trans*; 85.4% ±1.6 for 9-*cis*) and Chl *b* the lowest (59.4% ±4.5). The

471 ΣDoL was comparable for Lut (72.9% ±2.8) and Chl *a* (71.5% ±4.0). Notably, P13 showed

472 substantially lower ΣDoL for Chl *a* (ca. 18.9%) than for Lut (ca. 36.4%). Far below the values

473   of the ^{13}C-labeled plants, ΣDoL of the control plants ranged between 1.0% and 1.5% for all

474   pigments, as is expected from the 1.1% natural abundance of $^{13}CO_2$ in the atmosphere.

475   NLP (Fig. 9b) shows a mirror image of ΣDoL (Fig. 9a). As seen for ΣDoL, the NLP values

476   were similar in all ^{13}C-labeled plants but the three (P6, P13 and P15). After the 7-d labeling,

477   the average NLP of the 12 plants was no more than 9.9% ±2.2 for all-*trans*-β-Car and 10.8%

478   ±1.6 for 9-*cis*-β-Car (Fig. 9b). These values are about a half of Chl *a* (18.9% ±3.2) and Lut

479   (23.5% ±2.9) or 1/3 of Chl *b* (33.0% ±4.3). The smallest plant (P13) had the largest NLP for all

480   pigments, showing again a large difference between Chl *a* (ca. 70.7%) and Lut (ca. 60.3%).

481   Having seen the non-uniform ^{13}C enrichment patterns in different pigments of the ^{13}C-

482   labeled plants (Fig. 9), we made pairwise comparisons of NLP between the pigments (Fig. 10).

483   All four comparisons revealed a positive linear correlation but the slope of regression lines

484   differed. The slope was roughly one in the comparison between the two Chls, although NLP

485   was always smaller for Chl *a* than for Chl *b* (Fig. 10a). The correlation between the two

486   carotenoids had a slope of less than 0.9 (Fig. 10b), suggesting a smaller variation in Lut per unit

487   change in all-*trans*-β-Car. The Chl-carotenoid comparisons, i.e., Chl *a vs* all-*trans*-β-Car (Fig.

488   10c; slope ~0.8) and Chl *b vs* Lut (Fig. 10d; slope <0.7), indicated larger variations for Chls

489   than for carotenoids among the 15 plants. Yet, NLP was consistently smaller for carotenoids

490   than for Chls. The same comparisons made for ΣDoL (Additional file 1; Fig. A11) displayed

491   the same trends in the opposite direction.

492   The large variations in NLP and ΣDoL found between the non-labeled and ^{13}C-labeled plants

493   as well as between the non-stressed and stressed plants (Figs. 9, 10; Additional file 1; Fig. A11)

494   are in marked contrast to the similarity in their pigment composition (Fig. 3).

495

Discussion

Chamber for long-term $^{13}CO_2$ labeling

498    $^{13}CO_2$ labeling offers a means to trace the fate of carbon assimilated by photoautotrophic

499   organisms. After fixation into sugars, further metabolization can be detected by GC-MS, LC-

500   MS or NMR [20–22] to study the networks of carbon metabolism in plant tissues. The interest

501   in metabolic flux analysis has been growing in plant research, despite the challenges that are

502   inherent to multi-compartment cells and multicellular samples [23–26]. For instance, $^{13}CO_2$

503   pulse-chase experiments have been conducted for flux analysis of central metabolism in intact

504   leaves and whole Arabidopsis rosettes [27–31]. For short-term (seconds to minutes) labeling to

505   capture rapid ^{13}C incorporation and enrichment in primary metabolites, labeling chambers and

506   leaf cuvettes must have a small volume to ensure minimal time lag after switching between

507   ambient CO_2 and $^{13}CO_2$ [27–31]. Some chambers also allow instant quenching (flash-freezing)

508   to preserve metabolic state of the sample. Small labeling chambers and cuvettes were also used

509   to track ^{13}C down the plastidic 2*C*-methyl-D-erythritol-4-phosphate (MEP) pathway and

510   isoprene biosynthesis [32–36].

511     $^{13}CO_2$ labeling is an established approach in plant research to investigate phenomena that

512   develop over hours and days or even weeks and months. Ecological and ecophysiological

513   studies, such as investigation of above- and belowground carbon allocation in trees [37–40],

514   employ $\delta^{13}C$ measurements by isotope ratio mass spectrometer following *in situ* $^{13}CO_2$ labeling.

515   The $\delta^{13}C$ method can also be employed for laboratory experiments to trace metabolization and

516   translocation of ^{13}C-labeled assimilates [41]. When combined with hydroponic cultivation, dual

517   labeling with $^{13}CO_2$ and ^{15}N (in the form of $^{15}NH_4NO_3$, $^{15}NH_4{}^{15}NO_3$ or $K^{15}NO_3$ in nutrient

518   solution) enables simultaneous tracking of C and N allocation [41]. While ^{15}N feeding was

519   successfully applied to unveil leaf proteome turnover [2, 3], attempts are being made with $^{13}CO_2$

520   to concomitantly analyze turnover of metabolites and proteins [42, 43]. Chambers for long-term

521     $^{13}CO_2$ labeling typically have a large volume to treat multiple plants in parallel [41–44]. Even

522   an entire walk-in climate chamber can be used for $^{13}CO_2$ labeling [45], budget permitting. In

523   order to both monitor and control the conditions during the experiments, long-term labeling

524   chambers are often equipped with environmental sensors and control devices [41, 42, 44].

525   The choice of chamber design depends on research goals and available resources. Our

526   labeling chamber for long-term turnover analysis belongs to the latter type. It has a volume of

527   ca. 70 L for simultaneous labeling of up to 15 small plants and is furnished with temperature,

528   humidity, light and pressure sensors besides the IRGA for measuring [CO_2] (Figs. 1, 2). Due to

529   the low sensitivity of LI-840 for $^{13}CO_2$, a preliminary experiment with normal CO_2 was

530   necessary to establish a labeling protocol (Additional file 1; Figs. A5, A6). Not having [$^{13}CO_2$]

531   measurement is a major limitation of the current setup of the labeling chamber, which may

532   result in variable [$^{13}CO_2$] between experiments. This limitation can be removed in the future by

533   installing an IRGA or other instrument that can measure $^{13}CO_2$. One could also consider the use

534   of isotope ratio mass spectrometry (IRMS) to check the similarity or dissimilarity of ^{13}C

535   assimilation by the plants in different experiments. If a $^{13}CO_2$ gas analyzer is not available, as

536   was the case in thepresent work, flow rate protocols developed in normal CO_2 can be used to

537   provide the experimental conditions in $^{13}CO_2$ that are as close to the set values as possible. It is

538   then imperative that very similar plants be used in both CO_2 and $^{13}CO_2$ experiments (Additional

539   file 1; Fig. A2-A4). Also, the importance of homogenous conditions inside the chamber (Fig.

540   2a) cannot be stressed enough; environmental heterogeneity can have cumulative effects on

541 $^{13}CO_2$ labeling of plants (replicates) over a long period. In the labeling experiment, except for

542 the visibly stressed P6, P13 and P15, the other plants were similar in terms of visual phenotype

543 (Additional file 1; Fig. A3), pigment composition (Fig. 3) as well as NLP and ΣDoL (Fig. 9).

544 Although $[^{13}CO_2]$ was not measured in this study, our chamber and experimental protocols

545 apparently provided adequate conditions for long-term $^{13}CO_2$ labeling.

546

NLP of carotenoids

548 Similar ΣDoL and NLP values of the non-stressed plants (Fig. 9) underscore high

549 reproducibility (both technical and biological) of the methods. Whilst the number of unresolved

550 mass peaks was greater in the TQ-MS data than in the FTICR-MS data (Additional file 2; Tables

551 A3–A18), high pigment recovery and reproducibility of the TQ-MS system could be validated

552 (Additional file 2; Tables A1, A2). Below, we discuss NLP of carotenoids (Lut and β-Car) and

553 Chls (Chl *a* and Chl *b*) obtained by TQ-MS.

554 Previously we described a method of Lut isotopolog profiling in ^{13}C-labeled leaf pigment

555 extracts [14]. Using the method, NLP was calculated for Lut extracted from leaves of the 7-d

556 ^{13}C-labeled Arabidopsis plants (Fig. 9b). The data of the non-stressed plants are scattered

557 around the median, which was much lower than the NLP in the stressed plants. The deviations

558 between the TQ-MS-based and FTICR-MS-based NLP are <1 point for Lut, despite the

559 unresolved peaks in the TQ-MS data at *m/z* 569–571 and *m/z* 607–608 (Additional file 2; Tables

560 A8, A10) [14]. This is because none of the overlapping peaks belongs to the predominant ion

561 $[M+H–H_2O]^+$. The relative intensity ($BPI_{i(norm)}$) of the overlapping peaks is too low to affect

562 ΣDoL and NLP substantially. Moreover, the overlaps between $[M]^+$ and $[M+H]^+$ are of no

563 consequence to NLP when they appear within non-labeled or labeled peak cluster; only the peak

564 assignment of small overlaps between non-labeled and labeled isotopologs at *m/z* 569–571

565 affects the calculation of NLP. The relative intensity in this *m/z* region is no more than 3% of

566 the total, about a half of which is assigned to non-labeled $[M]^+$ and $[M+H]^+$ and the other half

567 to ^{13}C-labeled $[M+H–2H_2O]^+$ (Additional file 2; Table A9). When the abundance of the latter

568 diminishes in less strongly labeled samples (e.g. in experiments with shorter labeling), between-

569 cluster peak overlap will not be an issue for Lut.

570 Given that all ionization products must have the same ^{13}C labeling pattern, an alternative

571 way to analyze Lut data is to avoid overlapping peak regions altogether and use only $[M+H–$

572 $H_2O]^+$, which constitutes >80% of our Lut mass spectra (Fig. 6; Additional file 1; Fig. A9a–c).

573 The NLP values thus calculated are ca. 20.9% and 20.6%, respectively, for the FTICR-MS and

574 TQ-MS data shown in Additional file 2; Tables A9, A10, instead of ca. 21.0% and 21.9%

575 considering all four ions. Regardless of whether the calculation includes all ions or only [M+H–

576 H$_2$O]$^+$, similar NLP values can be obtained for Lut, with very minor differences between

577 FTICR-MS and TQ-MS. We note that peak assignment and calculation of DoL and NLP

578 basically follow the same procedures for all xanthophylls that are typically found in chloroplasts.

579   New in the present study is the assignment of β-Car and Chl isotopolog peaks to enable

580 turnover analysis of different pigments in the same sample. Two well-separated peak clusters

581 characterize the mass spectra of all-*trans*-β-Car in ^{13}C-labeled samples (Fig. 5c, d; Additional

582 file 1; Fig. A9d–f): a labeled cluster at around *m/z* 575-576 and a non-labeled cluster at around

583 *m/z* 536-537. The latter reflects the natural abundance of ^{12}C/^{13}C, as seen in the control (Fig.

584 5a, b) and predicted by the simulation (Additional file 1; Fig. A8). Since the unresolved mass

585 peaks of β-Car appear solely within non-labeled or labeled cluster, they should not affect the

586 calculation of NLP. Even so, TQ-MS slightly underestimated NLP of β-Car in the ^{13}C-labeled

587 sample (ca. –1.9 and –2.8 points for all-*trans*- and 9-*cis*-β-Car, respectively) compared to

588 FTICR-MS. The discrepancy between the two instruments declines to ca. 1.1 and 1.7 points

589 when NLP of the FTICR-MS data is calculated from the major [M+H]$^+$ ion alone, rather than

590 both [M]$^+$ and [M+H]$^+$ (Additional file 2; Table A5).

591   All-*trans*-β-Car is the predominant form of Car in PSII and PSI [11, 46]. While α-Car may

592 also be found in leaf pigment extracts, especially (but not only) in shade-tolerant species [47,

593 48], the α-Car level is typically low in Arabidopsis leaves. Strong light and heat can trigger *cis-*

594 *trans* isomerization in carotenoids [49, 50], which can be separated by C$_{30}$ reversed-phase

595 HPLC column [51, 52]. In the present study, we had moderate light and temperature conditions

596 in the labeling chamber (Additional file 1; Fig. A7a, b) and pigments were extracted in chilled

597 acetone under dim light. Still, 9-*cis*-β-Car and 9-*cis*-Neo were detected in all samples (Fig. 4a).

598 Formation of these 9-*cis* isomers was specific, as neither 13-*cis* and 15-*cis* isomers of β-Car and

599 Neo nor any *cis* isomers of Vio, Anthera and Lut were found. In fact, 9-*cis*-β-Car is a native

600 constituent of cytochrome b_6f complex [53–55]. Binding of 9-*cis*-Neo to PSII light-harvesting

601 antenna complexes is also well-established [56–59]. Interestingly, even though the two β-Car

602 isomers differ greatly in the concentration (Fig. 4a), their NLP values after the 7-d ^{13}CO$_2$

603 labeling were equally low (Fig. 9b).

604

605 NLP of Chls

606 The ^{13}C-labeled isotopolog peaks are more broadly distributed than non-labeled ones. This

607 broadening is particularly manifest in the mass spectra of Chls (Figs. 7c, d and 8c, d) consisting

608 of a porphyrin ring and a phytol side chain. At the center of porphyrin is Mg with three naturally

609   abundant isotopes (^{24}Mg, ^{25}Mg and ^{26}Mg), which, however, hardly broadens the mass spectra

610   of non-labeled Chls (Figs. 7a, b and 8a, b). The broadening of Chl mass spectra is therefore

611   solely ascribable to ^{13}C enrichment. In accordance, similarly broad mass spectra were reported

612   for ^{13}C-labeled pheophytin following the removal of Mg from ^{13}C-labeled Chl [60].

613   The peak cluster of ^{13}C-labeled Chls extends over a wide *m/z* region, with the strongly

614   labeled isotopologs (^{13}C$_{55}$ to ^{12}C$_{15}$^{13}C$_{40}$) accounting for a large part of ΣDoL (Additional file 2;

615   Tables A13, A14, A17 and A18). The labeled [M+H]$^+$ cluster is tailing off at lower *m/z*, as can

616   be recognized in Figs. 7 and 8 despite the partial overlap with non-labeled [M+K]$^+$ peaks. The

617   mass peaks in this low *m/z* region have been attributed to isotopologs having ^{13}C-labeld

618   porphyrin with non-labeled phytol or ^{13}C-labeled phytol with non-labeled porphyrin [60]. Our

619   Chl mass spectra revealed a small sub-cluster at around ^{12}C$_{35}$^{13}C$_{20}$ (*m/z* ~913 for Chl *a* and ~927

620   for Chl *b;* Figs. 7 and 8), corresponding to non-labeled porphyrin with ^{13}C-labeled phytol. The

621   existence of this sub-cluster is most evident in the absence of [M+K]$^+$ in the FTICR-MS data

622   of Chl *b* (Fig. 8c). In contrast, mass peak distribution was continuous for ^{13}C-labeled porphyrin

623   with non-labeled phytol, suggesting variable ^{13}C enrichment patterns of the porphyrin moiety

624   synthesized from glutamate.

625   Glutamate is rather slowly labeled by ^{13}CO$_2$ and also slowly unlabeled during subsequent

626   chase in ambient CO$_2$ [28, 41, 42]. In comparison, glyceraldehyde-3-phosphate and pyruvate,

627   the two precursors of plastidic isoprenoid biosynthesis via the MEP pathway leading to

628   carotenoids and phytol, are rapidly labeled by ^{13}CO$_2$ in illuminated leaves [28]. The Chl

629   molecules comprising labeled and non-labeled moieties are thought to arise from recycling of

630   de-esterified chlorophyllide and phytol [60]. By using radioactive ^{3}H-labeling, incorporation of

631   phytol in Chl and tocopherol has been demonstrated in Arabidopsis seedlings [61]. It should be

632   noted, however, that Chl molecules, which are "newly" synthesized from recycled

633   chlorophyllide and recycled phytol, will be indistinguishable from preexisting "old" molecules

634   based on their mass. Should such complete recycling occur, it would result in overestimation

635   of NLP. How often Chl molecules are recycled in leaves is unknown. According to our data

636   from the 7-d labeled Arabidopsis leaves, the relative abundance of isotopologs with labeled and

637   non-labeled moieties was 5–9% of the total Chl pool (Figs. 7 and 8; Additional file 2; Tables

638   A13, A14, A17 and A18). Similar values (<10%) were also found for pheophytin prepared from

639   Chl *a* of *Synechocystis* sp. PCC 6803 after 2-d labeling with ^{13}C-glucose and H^{13}CO$_3^-$ [60].

640   We were unable to resolve all peaks in the pigment mass spectra, in particular for Chls

641   (Additional file 2; Tables A11–A18). Higher resolving power than was used in this study would

642   be desirable for better peak assignment. The analysis of Chl mass spectra can be simplified

643 through Mg removal by weak acid treatment [60], although this will require separate sample

644 preparation and analysis for Chls and carotenoids. Formation of alkali metal adducts is a

645 common phenomenon for some compounds in positive ion mode. We estimated the

646 contribution of $[M+K]^+$ in the overlapping peak region of ^{13}C-labeled Chl mass spectra (Figs.

647 7c, d and Fig. 8d) based on the $[M+K]^+$:$[M+H]^+$ ratio found in the control (Figs. 7a, b and Fig.

648 8b). This ratio was highly reproducible in the mass spectra of the four control plants (±6–8%

649 SD for Chl a, ±4% SD for Chl b). We assumed that the ^{13}C-labeled plants had similar levels of

650 K (hence also similar $[M+K]^+$:$[M+H]^+$ ratios) in leaves. As K contents may vary in different

651 tissues, genotypes and species under different conditions, careful choice of control is essential

652 to estimate the relative intensity of $[M+K]^+$ peaks in this way. Additionally, the choice of

653 ionization technique can partly ameliorate the problem with alkali metal adducts [62]; in the

654 present study, APCI (in FTICR-MS) induced less alkali metal adduction than ESI did (in TQ-

655 MS) (Figs. 7 and 8).

656   The calculation based on $[M+H]^+$ of ^{24}Mg-Chl indicated ca. 18.8% and 20.7% NLP for Chl

657 a (by TQ-MS and FTICR-MS, respectively) and ca. 33.6% and 33.0% for Chl b (Additional

658 file 2; Tables A13, A14, A17 and A18). The discrepancy between the two instruments is

659 somewhat larger for Chl a (ca. 2.2 points) and β-Car (ca. 1.1 and 1.7 points for all-*trans* and 9-

660 *cis*) than for Chl b and Lut (<1 point). In view of the variations among the non-stressed replicate

661 plants shown in Fig. 9b, this level of under- or overestimation is within a tolerable range.

662

663 ## Different NLP of carotenoids and Chls

664 Cells synthesize new molecules as they grow. Growth-driven incorporation of ^{13}C strongly

665 dilutes NLP in long-term labeling experiments. After the 7-d ^{13}CO$_2$ labeling, all pigments had

666 larger NLP in the stressed plants (Fig. 9b) showing reduced growth (Additional file 1; Fig. A3b).

667 If growth is the only process that dilutes NLP and there is no change in pigment concentration,

668 the entire set of pigments is expected to show more or less the same decline in NLP. Yet, our

669 analysis revealed distinct NLP for carotenoids and Chls (Fig. 9b), suggesting different turnover

670 of these pigments.

671   Our previous studies using radioactive ^{14}CO$_2$ labeling have shown the turnover of Chl a and

672 all-*trans*-β-Car in mature leaves of Arabidopsis in the light [12, 13]. Both pigments had ^{14}C

673 incorporation already after 30-min pulse labeling, whereas Chl b and xanthophylls did not. The

674 rapid labeling of Chl a and all-*trans*-β-Car without changes in their concentration is indicative

675 of high turnover, presumably in connection with the D1 damage and repair [12, 13]. The D1

676 protein of PSII reaction center is known to undergo high turnover in illuminated leaves [6–8].

677 Some of the Chl *a* and all-*trans*-β-Car molecules, which are bound in the reaction center and
678 core complex of PSII [11], seem to be degraded and replaced by newly synthesized molecules
679 during the repair cycle. Between the two, all-*trans*-β-Car had a smaller NLP after the 7-d $^{13}CO_2$
680 labeling (Figs. 9b, 10c). This may be explained by different localization of these pigments;
681 while all-*trans*-β-Car is mostly bound to the core complexes of PSII and PSI [11, 46], Chl *a* is
682 universally found in all photosynthetic pigment-protein complexes. The proportion of
683 molecules undergoing turnover in PSII is thus larger for all-*trans*-β-Car than for Chl *a*.
684 Moreover, NLP of Chl *a* may be underestimated due to complete recycling of chlorophyllide
685 and phytol, should this happen. Analogously, lower NLP of Lut compared to Chl *b* (Figs. 9b,
686 10d), the two pigments that co-localize in light-harvesting antenna complexes [56–59, 63], may
687 be a sign of Chl recycling, although higher turnover of Lut cannot be ruled out. If 9-*cis*-β-Car
688 is specifically bound to cytochrome b_6f complex [53–55], the similar NLP values found for all-
689 *trans*- and 9-*cis*-β-Car (Fig. 9b) may imply medium turnover of 9-*cis*-β-Car in cytochrome b_6f,
690 i.e., not as high as all-*trans*-β-Car in PSII but higher than that in PSI. Yet, given the incomplete
691 chromatographic separation of all-*trans*- and 9-*cis*-β-Car (Fig. 4g), their mass spectra (Fig. 5;
692 Additional file 1; Fig. A10) may contain some signals from each other. Better separation is
693 needed to estimate NLP of the less abundant 9-*cis*-β-Car (Fig. 4a).
694

Conclusions

696 With these combined methods for long-term $^{13}CO_2$ labeling and parallel determination of
697 pigment concentration and NLP established, it is now possible to study photosynthetic pigment
698 turnover. While we did not do time course analysis, the results presented in Figs. 9 and 10 point
699 to distinct turnover rates of carotenoids and Chls. Future experiments, including the
700 xanthophyll-cycle pigments that were left out of the scope of this study, could throw light on
701 active maintenance and adjustment of photosynthetic pigments in leaves. Since changes in ^{13}C
702 enrichment can be analyzed in a wide range of compounds using appropriate MS methods,
703 long-term $^{13}CO_2$ labeling chamber, like the one described above, can facilitate investigations of
704 dynamic turnover of various metabolites and macromolecules in plants on a time scale of hours
705 to days.
706

711

Authors' contributions

SM designed the experiments. EK designed the labeling chamber. EK, AC and TH installed the sensors and other devices of the labeling chamber. AC made the computer program. AT-MB and SM tested the labeling chamber. AT-MB, BT and SM performed experiments and analyzed data. SM and AT-MB wrote the manuscript. All authors read and approved the final manuscript.

717

Funding

722

Availability of data and materials

The datasets obtained and/or analyzed during the current study are available from the corresponding author on request.

726

Declarations

Ethics approval and consent to participate

Not applicable.

730

Consent for publication

All authors affirm consent for publication.

733

Competing interests

The authors declare that they have no competing interests.

736

737

References

738

739 [1] Penning de Vries FWT. The cost of maintenance processes in plant cells. Ann Bot.
740   1975;39:77–92. https://doi.org/10.1093/oxfordjournals.aob.a084919.

741 [2] Nelson CJ, Alexova R, Jacoby RP, Millar AH. Proteins with high turnover rate in barley leaves
742   estimated by proteome analysis combined with in planta isotope labeling. Plant Physiol.
743   2014;166:91–108. https://doi.org/10.1104/pp.114.243014.

744 [3] Li L, Nelson CJ, Trösch J, Castleden I, Huang S, Millar AH. Protein degradation rate in
745   *Arabidopsis thaliana* leaf growth and development. Plant Cell. 2017;29:207–28.
746   https://doi.org/10.1105/tpc.16.00768.

747 [4] Chatterjee A, Abeydeera ND, Bale S, Pai P-J, Dorrestein PC, Russel DH, Ealick SE, Begley
748   TP. *Saccharomyces cerevisiae* THI4p is a suicide thiamine thiazole synthase. Nature.
749   2011;478:542–6. https://doi.org/10.1038/nature10503.

750 [5] Fitzpatrick TB, Chapman LM. The importance of thiamine (vitamin B_1) in plant health: From
751   crop yield to biofortification. J Biol Chem. 2020;295(34):12002–13.
752   https://doi.org/10.1074/jbc.REV120.010918.

753 [6] Murata N, Takahashi S, Nishiyama Y, Allakhverdiev SI. Photoinhibition of photosystem II
754   under environmental stress. Biochim Biophys Acta. 2007;1767:414–21.
755   https://doi.org/10.1016/j.bbabio.2006.11.019.

756 [7] Tikkanen M, Mekala NR, Aro E-M. Photosystem II photoinhibition-repair cycle protects
757   Photosystem I from irreversible damage. Biochim Biophys Acta. 2014;1837:210–5.
758   https://doi.org/10.1016/j.bbabio.2013.10.001.

759 [8] Li L, Aro E-M, Millar AH. Mechanisms of photodamage and protein turnover in photoinhibition.
760   Trends Plant Sci. 2018;23(8):667–76. https://doi.org/10.1016/j.tplants.2018.05.004.

761 [9] Raven JA. The cost of photoinhibition. Physiol Plant. 2011;142:87–104.
762   https://doi.org/10.1111/j.1399-3054.2011.01465.x.

763 [10] Miyata K, Noguchi K, Terashima I. Cost and benefit of the repair of photodamaged
764   photosystem II in spinach leaves: roles of acclimation to growth light. Photosynth Res.
765   2012;113:165–80. https://doi.org/10.1007/s11120-012-9767-0.

766 [11] Umena Y, Kawakami K, Shen J-R, Kamiya N. Crystal structure of oxygen-evolving
767   photosystem II at a resolution of 1.9 Å. Nature. 2011;473:55–60.
768   https://doi.org/10.1038/nature09913.

769 [12] Beisel KG, Jahnke S, Hofmann D, Köppchen S, Schurr U, Matsubara S. Continuous turnover
770   of carotenes and chlorophyll a in mature leaves of Arabidopsis revealed by $^{14}CO_2$ pulse-
771   chase labeling. Plant Physiol. 2010;152:2188–99. https://doi.org/10.1104/pp.109.151647.

772 [13] Beisel KG, Schurr U, Matsubara S. Altered turnover of β-carotene and Chl a in Arabidopsis
773   leaves treated with lincomycin or norflurazon. Plant Cell Physiol. 2011;52(7):1193–203.
774   https://doi.org/10.1093/pcp/pcr069.

775 [14] Thiele B, Matsubara S. Carotenoid isotopolog profiling in ^{13}C-labeled leaf extracts by LC-MS
776   and LC-FTICR-MS. In: Rodríguez-Concepción M, Welsch R, editors. *Plant and Food*
777   *Carotenoids: Methods and Protocols*, Methods in Molecular Biology. vol. 2083. New York:
778   Humana Press; 2020. p. 263–77. https://doi.org/10.1007/978-1-4939-9952-1_20.
779 [15] Jansen M, Gilmer F, Biskum B, Nagel KA, Rascher U, Fischbach A, et al. Simultaneous
780   phenotyping of leaf growth and chlorophyll fluorescence via GROWSCREEN FLUORO
781   allows detection of stress tolerance in *Arabidopsis thaliana* and other rosette plants. Funct
782   Plant BIol. 2009;36(11):902–14. https://doi.org/10.1071/FP09095.
783 [16] https://imagej.nih.gov/ij. Accessed 23 January 2019.
784 [17] Loreto F, Velikova V, Di Marco G. Respiration in the light measured by $^{12}CO_2$ emission in
785    $^{13}CO_2$ atmosphere in maize leaves. Aust J Plant Physiol. 2001;28:1003–8.
786   https://doi.org/10.1071/PP01091.
787 [18] van Breemen RB, Huang C-R, Tan Y, Sander LC, Schilling AB. Liquid chromatography/mass
788   spectrometry of carotenoids using atmospheric pressure chemical ionization. J Mass Spec.
789   1996;31:975-81.
790   https://doi.org/10.1002/(SICI)1096-9888(199609)31:9<975::AID-JMS380>3.0.CO;2-S.
791 [19] Řezanka T, Olšovská J, Sobotka M, Sigler K. The use of APCI-MS with HPLC and other
792   separation techniques for identification of carotenoids and related compounds. Curr Anal
793   Chem. 2009;5:1-25. https://doi.org/10.2174/157341109787047862.
794 [20] Kikuchi J, Shinozaki K, Hirayama T. Stable isotope labeling of *Arabidopsis thaliana* for an
795   NMR-based metabolomic approach. Plant Cell Physiol. 2004;45(8):1099–104.
796   https://doi.org/10.1093/pcp/pch117.
797 [21] Freund DM, Hegeman AD. Recent advances in stable isotope-enabled mass spectrometry-
798   based plant metabolomics. Curr Opin Biotechnol. 2017;43:41–8.
799   https://doi.org/10.1016/j.copbio.2016.08.002.
800 [22] Jang C, Chen L, Rabinowitz JD. Metabolomics and isotope tracing. Cell. 2018; 173:822–37.
801   https://doi.org/10.1016/j.cell.2018.03.055.
802 [23] Allen DK, Libourel IG, Shachar-Hill Y. Metabolic flux analysis in plants: coping with
803   complexity. Plant Cell Environ. 2009;32:1241–57.
804   https://doi.org/10.1111/j.1365-3040.2009.01992.x.
805 [24] Shih M-L, Morgan JA. Metabolic flux analysis of secondary metabolism in plants. Metab Eng
806   Commun. 2020;10:e00123. https://doi.org/10.1016/j.mec.2020.e00123.
807 [25] Wieloch T. The next phase in the development of ^{13}C isotopically non-stationary metabolic
808   flux analysis. J Exp Bot. 2021;72(18):6087-90. https://doi.org/10.1093/jxb/erab292.
809 [26] Kruger NJ, Ratchliffe RG. Whither metabolic flux analysis in plants? J Exp Bot. 2021.
810   https://doi.org/10.1093/jxb/erab389.
811 [27] Hasunuma T, Harada K, Miyazawa S-I, Kondo A, Fukusaki E, Miyake C. Metabolic turnover
812   analysis by a combination of in vivo ^{13}C-labelling from $^{13}CO_2$ and metabolic profiling with

CE-MS/MS reveals rate-limiting steps of the C_3 photosynthetic pathway in *Nicotiana tabacum* leaves. J Exp Bot. 2010;61(4):1041–51. https://doi.org/10.1093/jxb/erp374.

[28] Szecowka M, Heise R, Tohge T, Nunes-Nesi A, Vosloh D, Huege J, Feil R, Lunn J, Nikoloski Z, Stitt M, Fernie AR, Arrivault S. Metabolic fluxes in an illuminated *Arabidopsis* rosette. Plant Cell. 2013;25:694–714. https://doi.org/10.1105/tpc.112.106989.

[29] Ma F, Jazmin LJ, Young JD, Allen DK. Isotopically nonstationary ^{13}C flux analysis of changes in *Arabidopsis thaliana* leaf metabolism due to high light acclimation. Proc Natl Acad Sci USA. 2014;111(47):16967–72. https://doi.org/10.1073/pnas.1319485111.

[30] Arrivault S, Obata T, Szecówka M, Mengin V, Guenther M, Hoehne M, Fernie AR, Stitt M. Metabolite pools and carbon flow during C_4 photosynthesis in maize: $^{13}CO_2$ labeling kinetics and cell type fractionation. J Exp Bot. 2017;68(2):283–98. https://doi.org/10.1093/jxb/erw414.

[31] Abadie C, Tcherkez G. ^{13}C isotope labelling to follow the flux of photorespiratory intermediates. Plants. 2021;10:427. https://doi.org/10.3390/plants10030427.

[32] González-Cabanelas D, Wright LP, Paetz C, Onkokesung N, Gershenzon J, Rodríguez-Concepción M, Phillips MA. The diversion of 2-*C*-methyl-D-erythritol-2,4-cyclodiphosphate from the 2-*C*-methyl-D-erythritol 4-phosphate pathway to hemiterpene glycosides mediates stress responses in *Arabidopsis thaliana*. Plant J. 2015;82:122–37. https://doi.org/10.1111/tpj.12798.

[33] Bergman ME, González-Cabanelas D, Wright LP, Walker BJ, Phillips MA. Isotope ratio-based quantification of carbon assimilation highlights the role of plastidial isoprenoid precursor availability in photosynthesis. Plant Methods. 2021;17:32. https://doi.org/10.1186/s13007-021-00731-8.

[34] Delwiche CF, Sharkey TD. Rapid appearance of ^{13}C in biogenic isoprene when $^{13}CO_2$ is fed to intact leaves. Plant Cell Physiol. 1993;16:587–91. https://doi.org/10.1111/j.1365-3040.1993.tb00907.x.

[35] Karl T, Fall R, Rosenstiel TN, Prazeller P, Larsen B, Seufert G, Lindinger W. On-line analysis of the $^{13}CO_2$ labeling of leaf isoprene suggests multiple subcellular origins of isoprene precursors. Planta. 2002;215:894–905. https://doi.org/10.1007/s00425-002-0825-2.

[36] Ghirardo A, Wright LP, Bi Z, Rosenkranz M, Pulido P, Rodríguez-Concepción M, Niinemets Ü, Brüggemann N, Gershenzon J, Schnitzler J-P. Metabolic flux analysis of plastidic isoprenoid biosynthesis in poplar leaves emitting and nonemitting isoprene. Plant Physiol. 2014;165:37–51. https://doi.org/10.1104/pp.114.236018.

[37] Kagawa A, Sugimoto A, Maximov TC. Seasonal course of translocation, storage and remobilization of ^{13}C pulse-labeled photoassimilate in naturally growing *Larix gmelinii* saplings. New Phytol. 2006;171:793–804. https://doi.org/10.1111/j.1469-8137.2006.01780.x.

851 [38] Högberg P, Högberg MN, Göttlicher SG, Betson NR, Keel SG, Metcalfe DB, Campbell C,
852   Schindlbacher A, Hurry V, Lundmark T, Linder S, Näsholm T. High temporal resolution
853   tracing of photosynthate carbon from the tree canopy to forest soil microorganisms. New
854   Phytol. 2008;177:220–8. https://doi.org/10.1111/j.1469-8137.2007.02238.x.

855 [39] Epron D, Ngao J, Dannoura M, Bakker RM, Zeller B, Bazot S, Bosc A, Plain C, Lara J-C,
856   Priault P, Barthes L, Loustau D. Seasonal variations of belowground carbon transfer
857   assessed by in situ $^{13}CO_2$ pulse labelling of trees. Biogeosciences. 2011;8:1153–68.
858   https://doi.org/10.5194/bg-8-1153-2011.

859 [40] Kuptz D, Fleischmann F, Matyssek R, Grams TEE. Seasonal patterns of carbon allocation to
860   respiratory pools in 60-yr-old deciduous (*Fagus sylvatica*) and evergreen (*Picea abies*)
861   trees assessed via whole-tree stable carbon isotope labeling. New Phytol. 2011;191:160–
862   72. https://doi.org/10.1111/j.1469-8137.2011.03676.x.

863 [41] Dersch LM, Beckers V, Rasch D, Melzer G, Bolten C, Kiep K, Becker H, Bläsing OE, Fuchs
864   R, Ehrhardt T, Wittmann C. Novel approach for high-throughput metabolic screening of
865   whole plants by stable isotopes. Plant Physiol. 2016;171:25–41.
866   https://doi.org/10.1104/pp.15.01217.

867 [42] Chen W-P, Yang X-Y, Harms GL, Gray WM, Hegeman AD, Cohen JD. An automated growth
868   enclosure for metabolic labeling of *Arabidopsis thaliana* with ^{13}C-carbon dioxide – an *in vivo*
869   labeling system for proteomics and metabolomics research. Proteome Sci. 2011;9:9.
870   https://doi.org/10.1186/1477-5956-9-9.

871 [43] Ishihara H, Moraes TA, Arrivault S, Stitt M. Assessing protein synthesis and degradation
872   rates in *Arabidopsis thaliana* using amino acid analysis. Curr Protoc. 2021;1:e114.
873   https://doi.org/10.1002/cpz1.114.

874 [44] Huege J, Sulpice R, Gibon Y, Lisec J, Koehl K, Kopka J. GC-EI-TOF-MS analysis of in vivo
875   carbon-partitioning into soluble metabolite pools of higher plants by monitoring isotope
876   dilution after $^{13}CO_2$ labelling. Phytochemistry. 2007;68:2257–72.
877   https://doi.org/10.1016/j.phytochem.2007.03.026.

878 [45] Gleichenhagen M, Zimmermann BF, Herzig B, Janzik I, Jahnke S, Boner M, Stehle P,
879   Galensa R. Intrinsic isotopic ^{13}C labelling of polyphenols. Food Chem. 2013;141(3):2582–
880   90. https://doi.org/10.1016/j.foodchem.2013.05.070.

881 [46] Amunts A, Toporik H, Borovikova A, Nelson N. Structure determination and improved model
882   of plant photosystem I. J Biol Chem. 2010;285(5):3478–86.
883   https://doi.org/10.1074/jbc.M109.072645.

884 [47] Demmig-Adams B. Survey of thermal energy dissipation and pigment composition in sun and
885   shade leaves. Plant Cell Physiol. 1998;39(5):474–82.
886   https://doi.org/10.1093/oxfordjournals.pcp.a029394.

887 [48] Matsubara S, Krause GH, Aranda J, Virgo A, Beisel KG, Jahns P, Winter K. Sun-shade
888   patterns of leaf carotenoid composition in 86 species of neotropical forest plants. Funct
889   Plant Biol. 2009;36:20–36. https://doi.org/10.1071/FP08214.

890 [49] Ashikawa I, Miyata A, Koike H, Inoue Y, Koyama Y. Light-induced structural change of β-
891   carotene in thylakoid membranes. Biochemistry. 1986;25:6154–60.
892   https://doi.org/10.1021/bi00368a049.

893 [50] Milanowska J, Gruszecki WI. Heat-induced and light-induced isomerization of the xanthophyll
894   pigment zeaxanthin. J Photochem Photobiol B. 2005;80(3):178–86.
895   https://doi.org/10.1016/j.jphotobiol.2005.05.004.

896 [51] Sander LC, Epler Sharpless K, Craft NE, Wise SA. Development of engineered stationary
897   phases for the separation of carotenoid isomers. Anal Chem. 1994;66:1667–74.
898   https://doi.org/10.1021/ac00082a012.

899 [52] Emenhiser C, Simunovic N, Sander LC, Schwartz SJ. Separation of geometrical carotenoid
900   isomers in biological extracts using a polymeric C_{30} column in reversed-phase liquid
901   chromatography. J Agric Food Chem. 1996;44:3887–93.
902   https://doi.org/10.1016/0021-9673(95)00336-L.

903 [53] Zhang H, Huang D, Cramer WA. Stoichiometrically bound $β$-carotene in the cytochrome b_6f
904   complex of oxygenic photosynthesis protects against oxygen damage. J Biol Chem.
905   1999;274(3):1581–7. https://doi.org/10.1074/jbc.274.3.1581.

906 [54] Kurisu G, Zhang H, Smith JL, Cramer WA. Structure of the cytochrome b_6f complex of
907   oxygenic photosynthesis: Tuning the cavity. Science 2003;302:1009–14.
908   https://doi.org/10.1126/science.1090165.

909 [55] Malone LA, Qian P, Mayneord GE, Hitchcock A, Farmer DA, Thompson RF, Swainsbury
910   DJK, Ranson NA, Hunter CN, Johnson MP. Cryo-EM structure of the spinach cytochrome
911   b_6f complex at 3.6 Å resolution. Nature. 2019;575:535–9.
912   https://doi.org/10.1038/s41586-019-1746-6.

913 [56] Liu Z, Yan H, Wang K, Kuang T, Zhang J, Gui L, An X, Chang W. Crystal structure of spinach
914   major light-harvesting complex at 2.72 Å resolution. Nature. 2004;428:287–92.
915   https://doi.org/10.1038/nature02373.

916 [57] Caffarri S, Passarini F, Bassi R, Croce R. A specific binding site for neoxanthin in the
917   monomeric antenna proteins CP26 and CP29 of photosystem II. FEBS Lett.
918   2007;581:4704–10. https://doi.org/10.1016/j.febslet.2007.08.066.

919 [58] Pan X, Li M, Wan T Wang L, Jia C, Hou Z, Zhao X, Zhang J, Chang W. Structural insights
920   into energy regulation of light-harvesting complex CP29 from spinach. Nat Struct Mol Biol.
921   2011;18(3):309–15. https://doi.org/10.1038/nsmb.2008.

922 [59] Wei X, Su X, Cao P, Liu X, Chang W, Li M, Zhang X, Liu Z. Structure of spinach photosystem
923   II-LHCII supercomplex at 3.2 Å resolution. Nature. 2016;534:69–74.
924   https://doi.org/10.1038/nature18020.

925 [60] Vavilin D, Vermaas W. Continuous chlorophyll degradation accompanied by chlorophyllide
926   and phytol reutilization for chlorophyll synthesis in *Synechocystis* sp. PCC 6803. Biochim
927   Biophys Acta. 2007;1767:920–9. https://doi.org/10.1016/j.bbabio.2007.03.010.

928 [61] Ischebeck T, Zbierzak AM, Kanwischer M, Dörmann P. A salvage pathway for phytol
929   metabolism in *Arabidopsis*. J Biol Chem. 2006;281(5):24707.
930   https://doi.org/10.1074/jbc.M509222200.

931 [62] Holčapek M, Jirásko R, Lísa M. Basic rules for the interpretation of atmospheric pressure
932   ionization mass spectra of small molecules. J Chromatogr A. 2010;1217:3908–21.
933   https://doi.org/10.1016/j.chroma.2010.02.049.

934 [63] Croce R, van Amerongen H. Light-harvesting in photosystem I. Photosynth Res.
935   2013;116:153–66. https://doi.org/10.1007/s11120-013-9838-x.

936

937

938

Figure legends

940 **Fig. 1**. Schematic overview of the $^{13}CO_2$ labeling chamber. The devices to control CO_2

941 concentration (mass flow controller, MFC) and air humidity (dew point trap) are depicted along

942 with the sensors for CO_2 (infrared gas analyzer, IRGA), temperature, humidity, light intensity

943 and pressure. The colored background shows the chamber area (top view). The arrows indicate

944 the directions of air (or water) flow. The size of the arrows and the thickness of the lines

945 correspond to the inner diameter of tubing (polytetrafluoroethylene or metal).

946

947
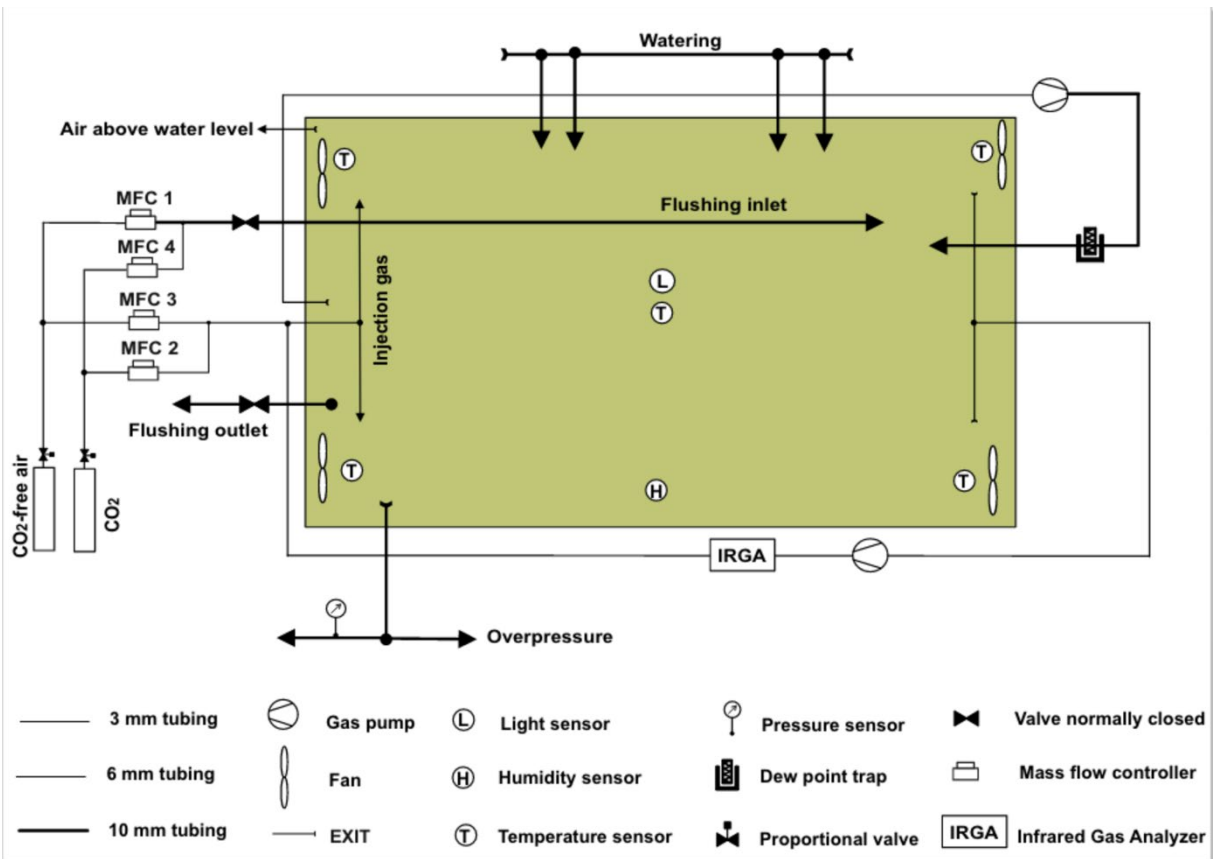
948 **Fig. 2**. Plant positions in the labeling chamber. **a** The positions of 15 plants (P1–P15) and the
949 light intensity (in µmol photon m^{-2} s^{-1}) distribution measured in and around each plant position
950 without the glass cover of the labeling chamber. The light intensity thus measured was ranging
951 between 204 (P15) and 279 (P7) µmol photon m^{-2} s^{-1} among the 15 positions, with the mean
952 intensity of 238 µmol photon m^{-2} s^{-1}. **b** A picture of the closed labeling chamber with 15
953 Arabidopsis plants placed under LED lamps in a controlled climate chamber. The bottom of the
954 plant cups (see Additional file 1; Fig. A1 for description of the plant cup) was touching the
955 water in a shallow basin attached to the lower surface of the chamber body. The basin can be
956 filled and drained through watering tubes (seen in the front) without opening the chamber.

957

958
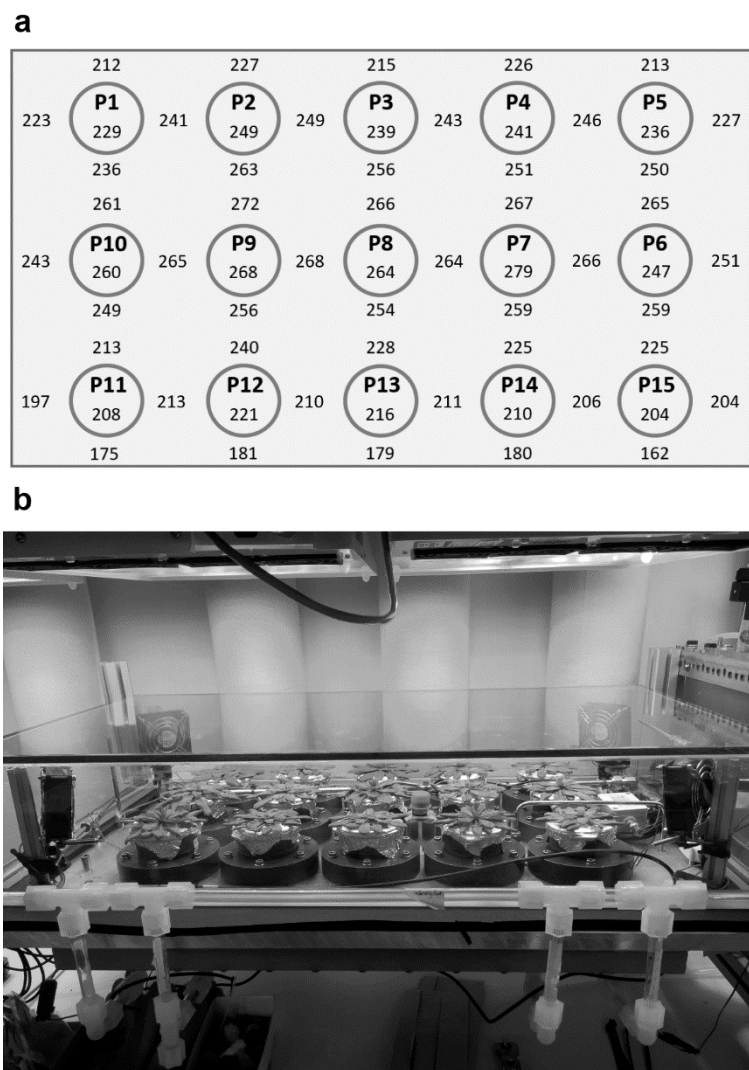
959 **Fig. 3**. Concentrations of photosynthetic pigments in Arabidopsis plants harvested in the early
960 morning of day 8. **a** Lutein (Lut) and all-*trans*-β-carotene (β-Car). **b** Zeaxanthin (Zea) and
961 antheraxanthin (Anthera). **c** Violaxanthin (Vio) and neoxanthin (Neo). Carotenoid levels
962 relative to the total chlorophyll content (mmol mol^{-1} Chl) are shown. **d** De-epoxidation state
963 (DES) of the xanthophyll cycle calculated as (Anthera + Zea)/(Vio + Anthera + Zea). **e**
964 Chlorophyll *a* (Chl *a*) and chlorophyll *b* (Chl *b*) contents per unit leaf mass (μmol g^{-1} fresh
965 weight). Black triangles represent control plants (*n*=4) that stayed in the ambient air outside the
966 labeling chamber. For ^{13}C-labeled samples, red and blue symbols are for plants with higher
967 (*n*=12) or lower (*n*=3) ^{13}C incorporation in the pigments, respectively. The latter showed visible
968 stress symptoms (see Additional file 1; Fig. A3b for images of the plants). The box plots are
969 based on all data. The thick horizontal line inside the box shows the median. The middle 50%
970 of the data fall between the upper and lower end of the box. Data beyond the whisker boundaries
971 are outliers.

972

973
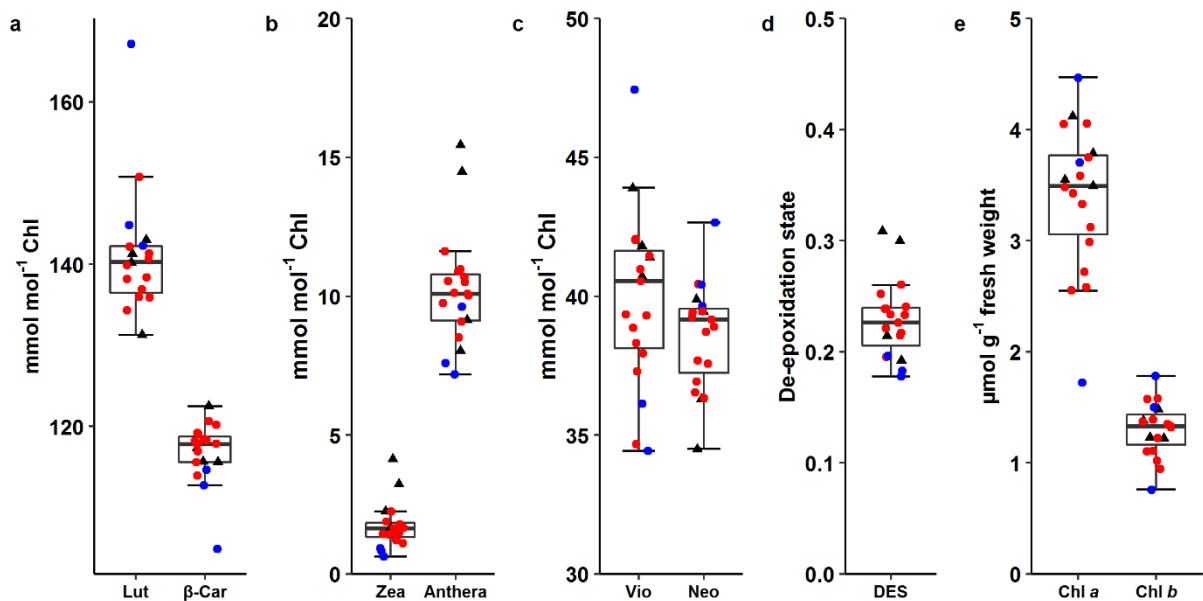
974   **Fig. 4**. Chromatograms of a ^{13}C-labeled Arabidopsis leaf pigment sample obtained by LC-TQ-

975   MS. **a** Pigment separation monitored at 440 nm. The pigment peaks are numbered as follows:

976   1, Vio; 2, 9-*cis*-Neo; 3, Anthera; 4, Chl *b*; 5, Lut; 6, Zea (if present); 7, Chl *a*; 8, all-*trans*-β-

977   Car; 9, 9-*cis*-β-Car. This sample had a very small amount of Anthera and hardly any Zea. In the

978   same sample, selected ions were monitored at specific mass-to-charge (*m/z*) values: **b** Vio and

979   9-*cis*-Neo; **c** Anthera; **d** Chl *b*; **e** Lut (and Zea if present); **f** Chl *a*; **g** all-*trans*- and 9-*cis*-β-Car.

980   Xanthophylls, especially Lut, tend to lose water upon protonation in positive ion mode.
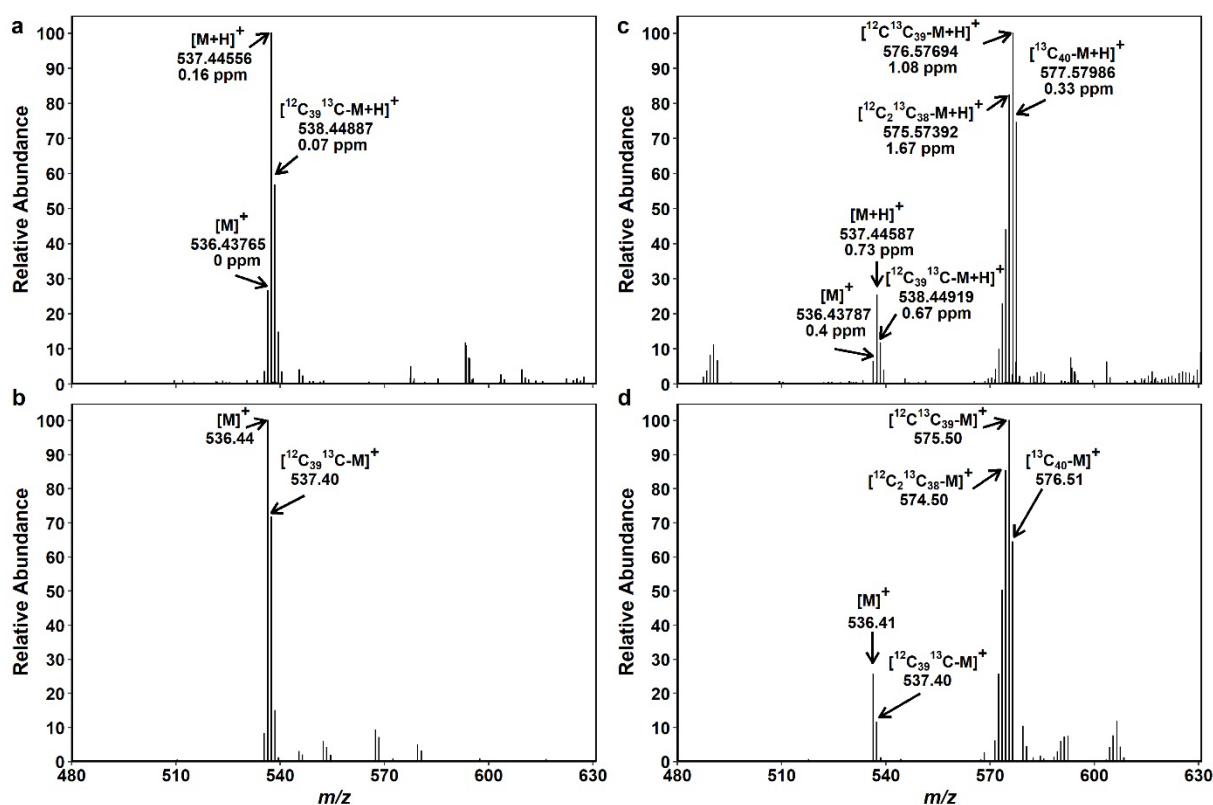
981

982
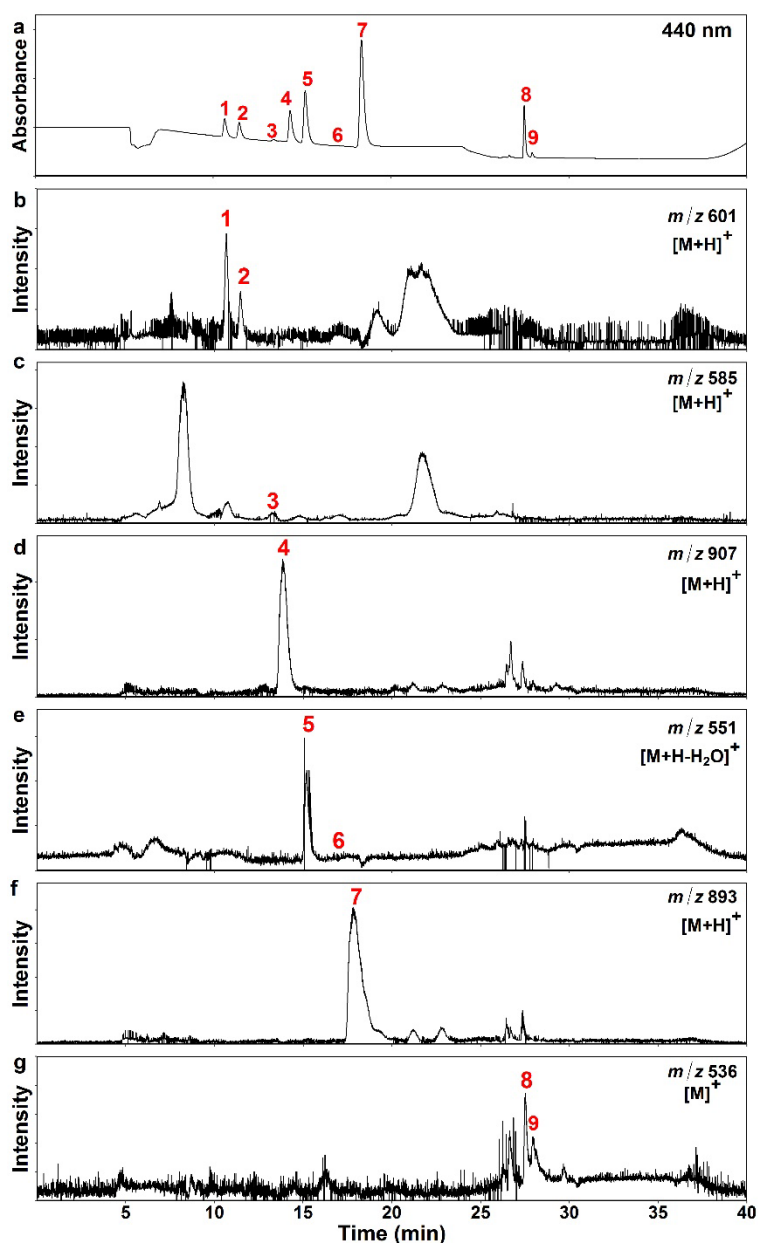
Fig. 5. Mass spectra of all-*trans*-β-Car extracted from non-labeled and ^{13}C-labeled Arabidopsis
plants. FTICR-MS showing two types of quasi-molecular ions of β-Car, $[M]^+$ and $[M+H]^+$, in
a non-labeled (**a**) and a ^{13}C-labeled (**c**) sample. Deviations from the expected mass (Δ) are given
in parts per million (ppm). TQ-MS in the same non-labeled (**b**) and ^{13}C-labeled (**d**) samples as
in **a** and **c**. Overlapping mass peaks of $[M]^+$ and $[M+H]^+$ ions are regarded as $[M+H]^+$ or $[M]^+$
in the analysis of FTICR-MS and TQ-MS, respectively. Peak assignment of these data is
summarized in Additional file 2; Tables A3–A6. Theoretical distribution of carotenoid
isotopologs based on natural ^{13}C abundance (~1.1%) is presented in Additional file 1; Fig. A8.

33

993 **Fig. 6**. Mass spectra of Lut extracted from non-labeled and ^{13}C-labeled Arabidopsis plants.

994 FTICR-MS showing four different types of quasi-molecular ions of Lut, $[M+H-2H_2O]^+$,

995 $[M+H-H_2O]^+$, $[M]^+$ and $[M+H]^+$, in a non-labeled (**a**) and a ^{13}C-labeled (**c**) sample. Small

996 peaks of ^{13}C-labeled $[M+H-2H_2O]^+$ ion were detected in the same m/z region as non-labelled

997 $[M]^+$ and $[M+H]^+$ ions in **c**. Deviations from the expected mass (Δ) are given in ppm. TQ-MS

998 showing four types of quasi-molecular ions, $[M+H-2H_2O]^+$, $[M+H-H_2O]^+$, $[M]^+$ and $[M+H]^+$,

999 in the same non-labeled (**b**) and ^{13}C-labeled (**d**) samples as in **a** and **c**. Since TQ-MS cannot

1000 separate overlapping peaks of non-labeled $[M]^+$ and $[M+H]^+$ at m/z 569–571 and ^{13}C-labeled

1001 $[M]^+$ and $[M+H]^+$ at m/z 607–608, they are regarded as $[M+H]^+$. Peak assignment of these

1002 data is summarized in Additional file 2; Tables A7–A10.
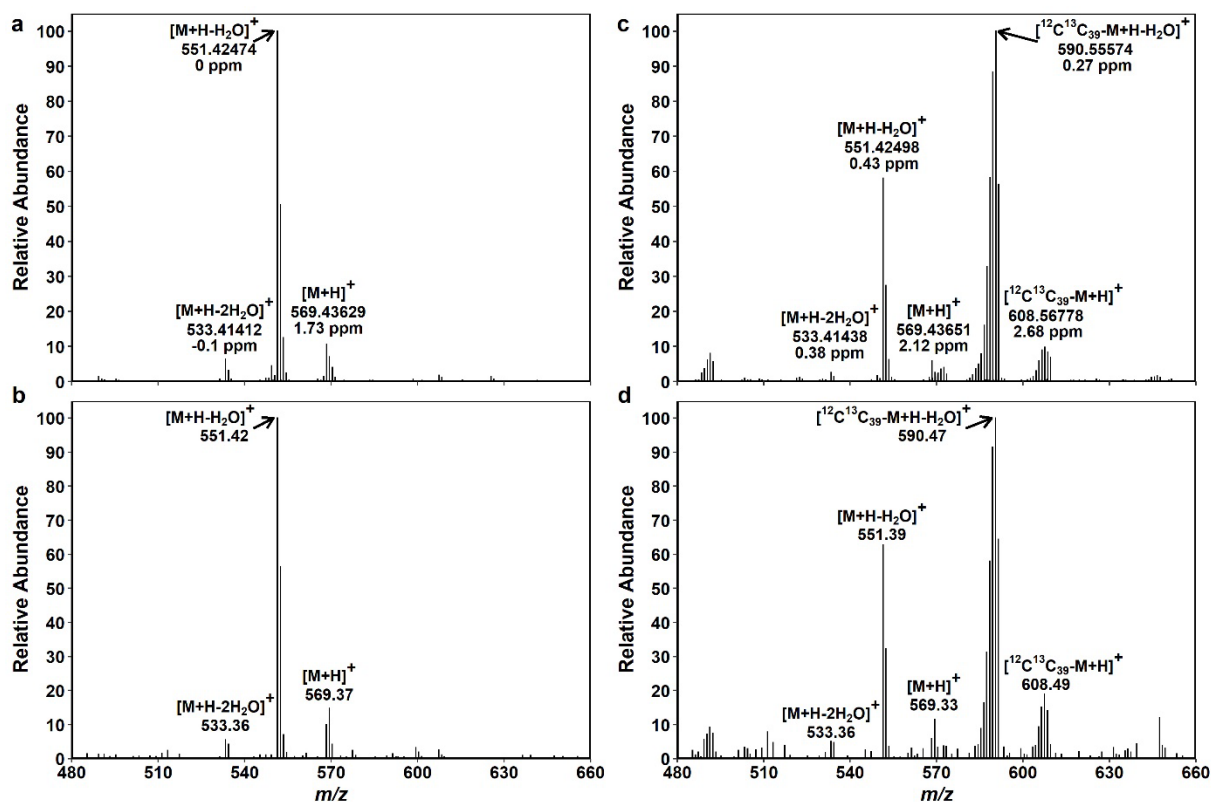
1003

1004

1005 **Fig. 7**. Mass spectra of Chl *a* extracted from non-labeled and ^{13}C-labeled Arabidopsis plants.
1006 FTICR-MS showing three types of quasi-molecular ions of Chl *a*, $[M]^+$, $[M+H]^+$ and $[M+K]^+$,
1007 in a non-labeled (**a**) and a ^{13}C-labeled (**c**) sample. Deviations from the expected mass (Δ) are
1008 given in ppm. TQ-MS showing two types of quasi-molecular ions, $[M+H]^+$ and $[M+K]^+$, in the
1009 same non-labeled (**b**) and ^{13}C-labeled (**d**) samples as in **a** and **c**. The $[M]^+$ peak was hardly
1010 detected and thus not considered in the analysis of TQ-MS data. Mass peaks of ^{13}C-labeled
1011 $[M+H]^+$ and non-labeled $[M+K]^+$ were overlapping at *m/z* 931–933 in **d**. The contribution of
1012 non-labeled $[M+K]^+$ in this *m/z* region was estimated from the intensity of non-labeled $[M+H]^+$
1013 peaks and the ratio between $[M+H]^+$ and $[M+K]^+$ peaks found in **b** (1:0.26). For Chl, natural
1014 abundance of Mg isotopes (^{24}Mg 79%, ^{25}Mg 10% and ^{26}Mg 11%) was taken into account to
1015 calculate their contributions to each mass peak. The estimated peak intensity of ^{24}Mg-Chl as
1016 $[M+H]^+$ was then considered representative of Chl *a* in the analysis of TQ-MS data. Peak
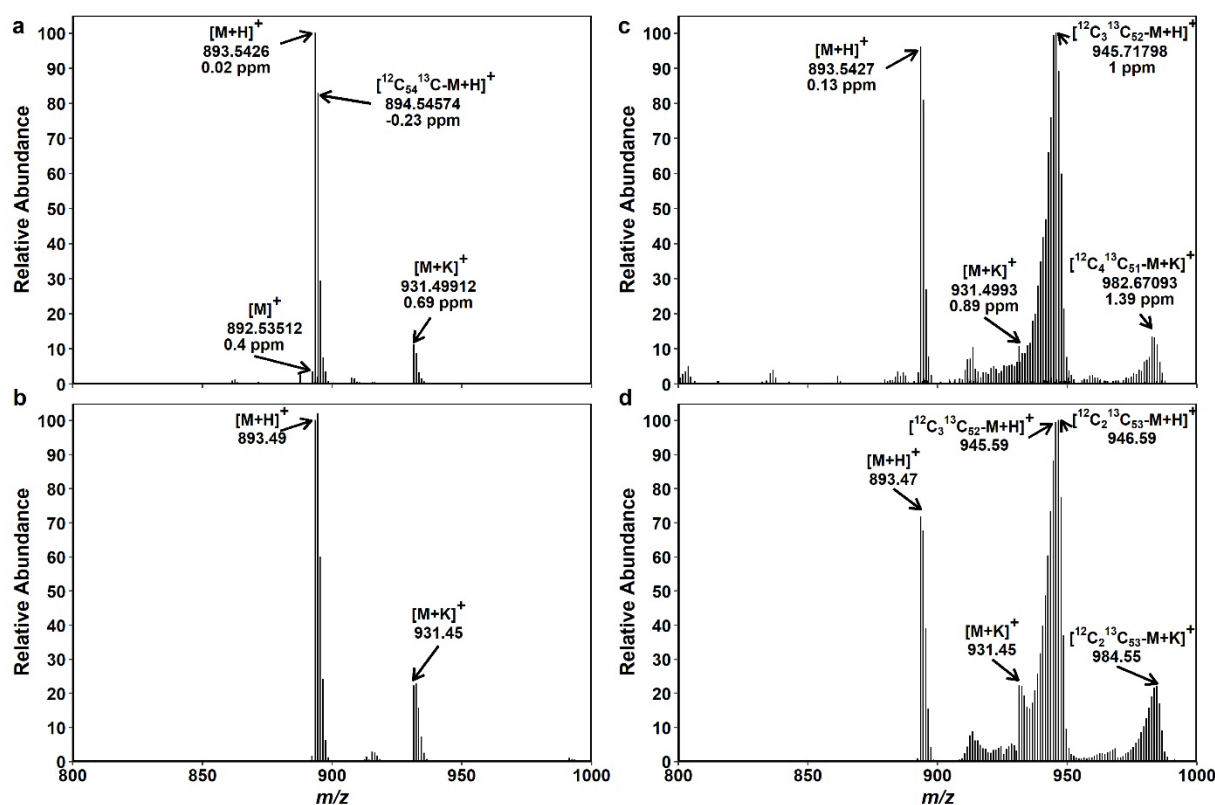1017 assignment of these data is summarized in Additional file 2; Tables A11–A14.

1018

1019

1020 **Fig. 8**. Mass spectra of Chl *b* extracted from non-labeled and ^{13}C-labeled *Arabidopsis* leaves.

1021 FTICR-MS showing two types of quasi-molecular ions of Chl *b*, $[M]^+$ and $[M+H]^+$, in a non-

1022 labeled (**a**) and a ^{13}C-labeled (**c**) sample. Deviations from the expected mass (Δ) are given in

1023 ppm. TQ-MS showing two types of quasi-molecular ions, $[M+H]^+$ and $[M+K]^+$, in the same

1024 non-labeled (**b**) and ^{13}C-labeled (**d**) samples as in **a** and **c**. The $[M]^+$ peak was hardly detected

1025 and thus not considered in the analysis of TQ-MS data. Mass peaks of ^{13}C-labeled $[M+H]^+$ and

1026 non-labeled $[M+K]^+$ were overlapping at *m/z* 945–948 in **d**. The contribution of non-labeled

1027 $[M+K]^+$ in this *m/z* region was estimated from the intensity of non-labeled $[M+H]^+$ peaks and

1028 the ratio between $[M+H]^+$ and $[M+K]^+$ peaks found in **b** (1:0.74). For Chl, natural abundance

1029 of Mg isotopes (^{24}Mg 79%, ^{25}Mg 10% and ^{26}Mg 11%) was taken into account to calculate their

1030 contributions to each mass peak. The estimated mass peak intensity of ^{24}Mg-Chl as $[M+H]^+$

1031 was then considered representative of Chl *b* in the analysis of TQ-MS data. Peak assignment of

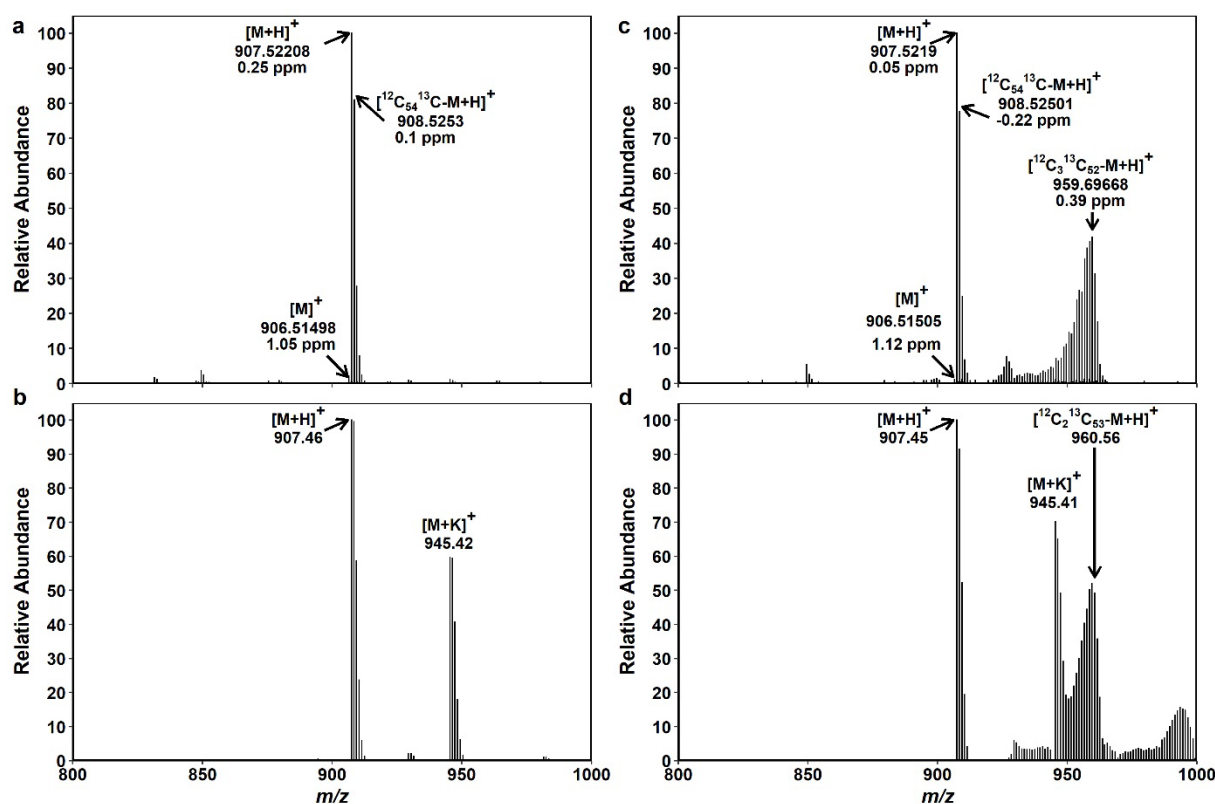1032 these data is summarized in Additional file 2; Tables A15-A18.

1033

1034

1035 **Fig. 9**. Labeled and non-labeled pigments in ^{13}C-labeled Arabidopsis leaves harvested after 7-
1036 d $^{13}CO_2$ labeling. **a** Degree of ^{13}C labeling (ΣDoL) and **b** non-labeled pigment population (NLP)
1037 of all-*trans*- and 9-*cis*-β-Car, Lut, Chl *a* and Chl *b*. Red and blue symbols represent plants that
1038 had higher (*n*=12) or lower (*n*=3) ^{13}C incorporation in pigments, respectively. Black triangles
1039 in **a** are control plants (*n*=4) that stayed in the ambient air outside the labeling chamber. Data
1040 of the control plants are not shown in **b** since they all had 100% NLP. The box plots are based
1041 on the data of the ^{13}C-labeled samples (i.e., red and blue symbols); the control plants (black
1042 triangles) shown in **a** are not included in the box plots. The thick horizontal line inside the box
1043 shows the median. The middle 50% of the data fall between the upper and lower end of the box.
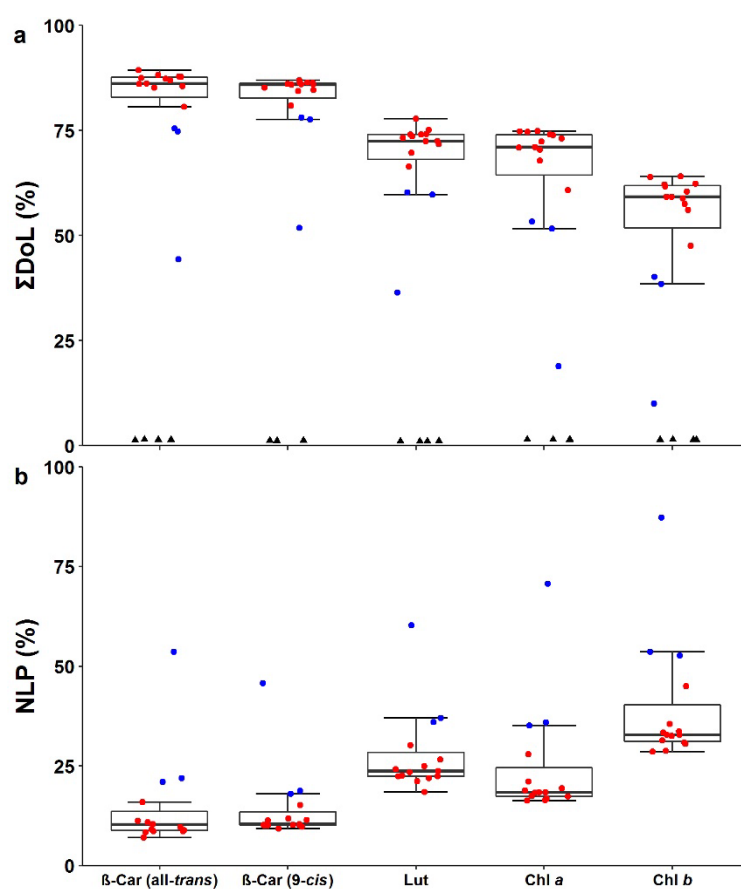1044 Data beyond the whisker boundaries are outliers.

1045

1046

1047

37

1048 **Fig. 10**. Correlation between non-labeled population (NLP) of pigments extracted from
1049 Arabidopsis leaves after 7-d $^{13}CO_2$ labeling. **a** Chl *a* and Chl *b*. **b** All-*trans*-β-Car and Lut. **c**
1050 Chl *a* and all-*trans*-β-Car. **d** Chl *b* and Lut. Red and blue symbols represent plants that had
1051 higher (*n*=12) or lower (*n*=3) ^{13}C incorporation in pigments, respectively.
1052

1053

1054